Reheating constraints on *k*-inflation

Pooja Pareek and Akhilesh Nautiyal
Department of Physics, Malaviya National Institute of Technology, Jaipur, JLN Marg, Jaipur 302017, India

(Received 17 March 2021; accepted 20 September 2021; published 13 October 2021)

In this work we revisit constraints on *k*-inflation with a Dirac-Born-Infeld (DBI) kinetic term and a power-law kinetic term from reheating. For the DBI kinetic term we choose monomial potentials, $V \propto \phi^n$ with $n = 2/3$, 1, 2, and 4, and natural inflaton potential, and for the power-law kinetic term we choose quadratic, quartic, and exponential potentials. The phase of reheating can be parametrized in terms of the reheating temperature, T_{re}, the number of e-folds during reheating N_{re}, and the effective equation of state during reheating w_{re}. These parameters can be related to the spectral index n_s and other inflationary parameters depending on the choice of inflaton kinetic term and potential. By demanding that w_{re} should have a finite range and T_{re} should be above the electroweak scale, one can obtain bounds on n_s that can provide bounds on the tensor-to-scalar ratio, r. We find, for *k*-inflation with a DBI kinetic term, and quadratic and quartic potentials, that the upper bound on r for the physically plausible value of $0 \leq w_{re} \leq 0.25$ is slightly larger than the *Planck* 2018 and BICEP2/Keck array bound, and for $n = 2/3$ and 1, the reheating equation of state should be less than 0 to satisfy *Planck* 2018 joint constraints on n_s and r. However, natural inflation with the DBI kinetic term is compatible with *Planck* 2018 bounds on r and joint constraints on n_s and r for the physically plausible range $0 \leq w_{re} \leq 0.25$. The quadratic and quartic potential with a power-law kinetic term are also compatible with *Planck* 2018 joint constraints on n_s and r for $0 \leq w_{re} \leq 1$. However, for an exponential potential with a power-law kinetic term, the equation of state during reheating, w_{re}, should be greater than 1 for $r - n_s$ predictions to lie within 68% C.L. of joint constraints on n_s and r from *Planck* 2018 observations.

DOI: 10.1103/PhysRevD.104.083526

I. INTRODUCTION

The idea of inflation [1] is now a well-accepted solution to the horizon and flatness problem of big bang cosmology. It also provides seeds for anisotropy of cosmic microwave background and structures in the Universe [2–4]. The predictions of inflation, i.e., nearly scale-invariant, Gaussian and adiabatic density perturbations are confirmed by the various cosmic microwave background (CMB) observations such as COBE [5] WMAP [6], *Planck* [7] etc. In the standard scenario the potential energy of a scalar field, named as inflaton, dominates the energy density of the Universe during inflation and provides quasiexponential expansion. Inflaton rolls slowly through its potential during inflation, and the quantum fluctuations in this field, which are coupled to the metric fluctuations, generate the primordial density perturbations (scalar perturbations). The vacuum fluctuations in the tensorial part of the metric generated during inflation are responsible for the primordial gravitational waves (tensor perturbations). The power spectra for scalar and tensor perturbations generated during inflation depend on the inflaton potential, which can be obtained from particle physics models and string theory. Many models of inflation have been explored in recent years (see [8] for details). Although the predictions of inflation are in excellent agreement with the CMB observations, we still lack a unique model. The most popular quadratic and quartic potentials are ruled out by recent *Planck* observations [7] as they give a large tensor to scalar ratio.

There is an alternative to the standard scenario of inflation, named as *k*-inflation [9,10], where inflation is achieved by the nonstandard kinetic term of the inflaton. The nonstandard kinetic term in the action of the inflaton can have monomial and polynomial forms [9,11] or a Dirac-Born-Infeld (DBI) form [12], which arises in string theory [13–16] (see [17–20] for various choices of non-cannonical kinetic terms and potentials derived from string theory). In [21–23] it was shown that the tensor to scalar ratio can be lowered for quadratic and quartic potentials with a noncanonical kinetic term. *k*-inflation with the pseudo-Nambu-Goldstone boson (PNGB) has also been studied in [21,24,25] and it was shown that natural inflation with a noncanonical kinetic term is compatible with the *Planck* and CMB observations. Power-law kinetic terms with an exponential potential have also been studied in [23] and it was found that this model is also compatible with the CMB observations. In [26] the power-law kinetic term has also been studied with deformed steepness exponential potentials.

Several generalizations of k-inflation have been studied in the literature such as the inflaton with nonminimal coupling with Ricci scalar [27,28], the inflaton coupled with Gauss-Bonnet invariant [29], and k-inflation with $f(R)$ gravity [30]. k-inflation with constant-roll conditions has also been studied in [31]. It has been shown in [32] that the action of R^2-inflation in the framework of Palatini gravity resembles k-inflation models in the Einstein frame.

All these models of noncanonical inflation are in agreement with the current bounds on the spectral index and the tensor to scalar ratio from *Planck* 2018 observations, and there is no unique choice for noncanonical kinetic term and inflaton potential.

At the end of inflation, the Universe reaches a cold and highly nonthermal state without any matter content. However, for baryogenesis and big bang nucleosynthesis the Universe needs to be in a thermalized state at a very high temperature. This is achieved by reheating a transition phase between the end of inflation and start of the radiation dominated era. During this phase the inflaton energy is transferred to radiation, baryons, and leptons, leaving the Universe at a reheating temperature T_{re} at the onset of radiation epoch. In the simplest models of reheating [33–35] inflaton oscillates around the minimum of its potential and decays perturbatively into the standard model particles through various interactions of inflaton with other scalars and fermions. However, perturbative reheating is model dependent and cannot give a correct description of the process at various states; it also does not take into account the coherent nature of the inflaton field [36,37]. In other scenarios the reheating is preceded by preheating, during which the classical inflaton field decays into massive particles via nonperturbative processes such as parametric resonance [38,39], tachyonic instability [40,41], and instant preheating [42]. After preheating these massive particles decay perturbatively into the standard model particles, which are then thermalized and the Universe enters into radiation dominated era with a blackbody spectrum at a temperature T_{re}, called the reheating temperature.

Although the physical processes involved during reheating are complex, this phase can be parametrized in terms of three parameters; reheating temperature T_{re}, the effective equation of state of matter during reheating w_{re}, and duration of reheating that is given in terms of the number of e-foldings N_{re}. The reheating temperature cannot be constrained from CMB and LSS observations, but it is assumed that T_{re} should be above the electroweak scale so that weak-scale dark matter can be produced. In a more conservative approach T_{re} should be above 10 MeV for successful big bang nucleosynthesis. The reheating temperature can be as low as 2.5 MeV to 4 MeV, for late-time entropy production by massive particle decay [43,44]. By considering instant reheating we can also put an upper bound on the reheating temperature T_{re} to be of the order of the scale of inflation, which is 10^{16} GeV for current upper bounds on tensor to scalar ratio from *Planck*. The second parameter of reheating is an effective equation of state w_{re} representing the evolution of energy density of the cosmic fluid during reheating. This parameter is, in general, time dependent and its value changes from $-\frac{1}{3}$ to $\frac{1}{3}$ from the end of inflation to the onset of the radiation dominated era. For reheating occurring due to the perturbative decay of the massive inflaton, w_{re} is 0 and for instant reheating it is $\frac{1}{3}$. The evolution of the equation of state during preheating and the early thermalization state was studied in [45] by using lattice numerical simulation for quadratic potential interacting with light fields, and it was found that the equation of state starts from $w_{re} = 0$ after inflation and saturates around $w_{re} \sim 0.2$–0.3 long before the thermalization of the Universe. This analysis was generalized in [46,47] for inflaton potentials behaving as $|\phi|^{2n}$ near $|\phi| = 0$, and flatter beyond some scale $|\phi| = M$ by taking into account the fragmentation of the inflaton field and ignoring coupling to massless fields. It was found that the equation of state w_{re} reaches $1/3$ for $n > 1$ after a sufficiently long time, while it remains 0 for $n = 1$. The third parameter needed to describe reheating is its duration which can be defined in terms of number of e-foldings from the end of inflation to the beginning of the radiation dominated epoch. This duration is incorporated in the number of e-foldings N_k during inflation from the time, when the Fourier mode k corresponding to the horizon size of the present observable Universe leaves the Hubble radius during inflation, to the end of inflation. The e-foldings N_k depend on the potential of inflaton and it should be between 46 to 70 to solve the horizon problem. The upper bound on N_k arises from assuming that the Universe reheats instantaneously, and the lower bound comes from considering the reheating temperature at the electroweak scale. In [48,49] a detailed analysis of the upper bound on N_k that we performed for various scenarios it was shown that, for some cases, N_k can be as large as 107.

In [50–52] it was shown that the above mentioned reheating parametrization can be used to constrain various models of inflation. The reheating temperature T_{re} and the e-folds during reheating N_{re} can be expressed in terms of spectral index n_s by assuming w_{re} is constant during reheating [50–52]. By imposing that the effective equation of state during reheating lies between 0 and 0.25 and the temperature at the end of reheating is $T > 100$ GeV, one can obtain bounds on spectral index n_s and N_k, which translates to bounds on tensor to scalar ratio. As various models of inflation predict similar values of n_s and r, it has been shown in [53] that by imposing constraints on these reheating parameters this degeneracy can be removed. The bounds on reheating parameters were also used to constrain tachyon inflation [54], where inflaton has a DBI kinetic term with inverse cosh and exponential potential. It was shown that one requires an effective equation of state during reheating $w_{re} > 1$ to satisfy the *Planck* 2018 observations.

In this work we use these reheating parameters to constrain k-inflation with a DBI kinetic term, monomial potentials, PNGB potential, and k-inflation with a power-law kinetic term with monomial and exponential potentials. Reheating constraints on noncanonical inflation with inflatons having a DBI kinetic term and PNGB potential are already considered in [24] using *Planck* 2015 data. Here we revisit tachyon natural inflation with *Planck* 2018 data along with other potentials with a DBI kinetic term.

The work is organized as follows. In Sec. II we discuss the dynamics of k-inflation and present expressions for power spectra. In Sec. III we discuss the parametrization of the reheating phase. We obtain expressions for T_{re} and N_{re} in terms of the spectral index by assuming a constant effective equation of state during reheating. In Sec. IV we discuss noncanonical inflation with a DBI kinetic term and obtain expressions for T_{re} and N_{re} for monomial and PNGB potential for various choices for w_{re}. We use these three parameters to constrain k-inflation with a DBI kinetic term. In Sec. V we discuss dynamics of noncanonical inflation with a power law kinetic term, and obtain T_{re} and N_{re} for monomial and exponential potential with various choices of w_{re}. We again use these three parameters to constrain k-inflation with a power-law kinetic term. In Sec. VI we conclude our work.

II. k-INFLATION: General framework

In k-inflation the inflaton field has a noncanonical kinetic term. The action for inflaton is given as

$$S = \int \sqrt{-g}\left\{-\frac{1}{16\pi G}R + \mathcal{L}(X,\phi)\right\}, \tag{1}$$

where $\mathcal{L}(X,\phi)$ is the Lagrangian of scalar field, which is a function of the kinetic term $X = \frac{1}{2}\partial_\mu\phi\partial^\mu\phi$ and the field ϕ. We can obtain the energy-momentum tensor by varying this action with respect to the metric as

$$T_{\mu\nu} = \frac{\partial\mathcal{L}(X,\phi)}{\partial X}\partial_\mu\phi\partial_\nu\phi - \mathcal{L}(X,\phi)g_{\mu\nu}. \tag{2}$$

This energy-momentum tensor is equivalent to that of a perfect fluid with pressure

$$p = \mathcal{L}(X,\phi), \tag{3}$$

energy density

$$\rho = 2X\frac{\partial\mathcal{L}}{\partial X} - \mathcal{L}, \tag{4}$$

and four-velocity

$$u_\mu = \sigma\frac{\partial_\mu\phi}{\sqrt{2X}}, \tag{5}$$

where σ refers to the sign of $\dot{\phi}$. The evolution of the Universe is described using the Friedmann equations

$$H^2 = \frac{1}{3M_P^2}\rho, \tag{6}$$

$$\dot{H} = -\frac{1}{2M_P^2}(\rho + p). \tag{7}$$

Here $M_P = \frac{1}{\sqrt{8\pi G}}$ is the reduced Planck mass. For inflation the second derivative of the scale factor should satisfy the condition $\frac{\ddot{a}}{a} = \dot{H} + H^2 > 0$, which can be expressed in terms of the slow-roll parameter

$$\epsilon = -\frac{\dot{H}}{H^2} < 1. \tag{8}$$

For our analysis we define slow-roll parameters in terms of the Hubble flow parameters as [55]

$$\epsilon_0 \equiv \frac{H_k}{H}, \tag{9}$$

and

$$\epsilon_i \equiv \frac{d\,\ln|\epsilon_i|}{dN}, \quad i \geq 0, \tag{10}$$

where H_k is the Hubble constant during inflation at the time when a particular mode k leaves the horizon and N is the number of e-foldings

$$N = \ln\left(\frac{a}{a_i}\right), \tag{11}$$

where a_i is the scale factor at the beginning of inflation. The first derivative of the Hubble flow parameter with respect to time can be expressed as

$$\dot{\epsilon}_i = \epsilon_i\epsilon_{i+1}. \tag{12}$$

The first two Hubble flow parameters ϵ_1 and ϵ_2 can be obtained in terms of energy density and pressure as

$$\epsilon_1 = \epsilon = \frac{3}{2}\frac{\rho + p}{\rho}, \tag{13}$$

$$\text{and} \quad \epsilon_2 = \frac{3}{2H}\frac{d}{dt}\left(\frac{\rho + p}{\rho}\right). \tag{14}$$

The power spectra for scalar and tensor perturbations, scalar spectral index n_s, and tensor to scalar ratio r for k-inflation are computed in [10], and can be expressed in terms of the Hubble flow parameters as

$$P_\zeta = \left.\frac{H^2}{8\pi^2 M_P^2 c_s \epsilon}\right|_{c_S k = aH}, \tag{15}$$

$$P_h = \frac{2}{\pi^2}\frac{H^2}{M_P^2}|_{c_S k = aH}, \tag{16}$$

$$n_s = 1 - 2\epsilon_1 - \epsilon_2, \tag{17}$$

$$r = 16 c_S \epsilon_1, \tag{18}$$

where

$$c_S^2 = \frac{\partial p/\partial X}{\partial \rho/\partial X} \tag{19}$$

is the sound speed for perturbations. These power spectra are evaluated at the Hubble crossing during inflation for the Fourier mode k of curvature perturbation and tensor perturbation. In k-inflation the condition for Hubble exit is modified as $c_S k = aH$ for scalar perturbations. For CMB analysis the power spectrum for curvature perturbation is expressed as $P_\zeta = A_S(\frac{k}{k_0})^{n_s - 1}$, where the amplitude of scalar perturbations A_S is given by Eq. (15). All the three quantities A_S, n_s, and r are evaluated at pivot scale k_0, which is 0.05 $\mathrm{M_{pc}}^{-1}$ for Planck observations, and they depend on the choice of noncanonical kinetic terms and the potential of inflaton. Bounds on these quantities are provided by CMB and LSS observations, which can be used to put constraints on parameters of the potential and the noncanonical kinetic term of inflaton. Again all these inflationary parameters also appear in the reheating temperature and number of e-folds during reheating, which can, along with CMB constraints, be used to analyze models of inflation. In this work we analyze k-inflation having a noncanonical kinetic term of DBI form in section and power-law form. In the next section we obtain a relationship between reheating parameters, T_{re} and N_{re}, and inflationary parameters.

III. PARAMETRIZING REHEATING

As mentioned earlier, the reheating phase can be parametrized in terms of thermalization temperature T_{re} at the onset of the radiation dominated epoch after reheating, effective equation of state of cosmic fluid w_{re} during reheating, and the number of e-folds N_{re} for which reheating lasts. In our analysis we consider w_{re} to be constant during reheating. Its value should lie between $-\frac{1}{3}$ to 1. The lower bound on w_{re} comes from the fact that it should be $-\frac{1}{3}$ when inflation ends, and the upper bound arises from the fact that it should be smaller than 1 to satisfy the dominant energy condition of general relativity, $\rho \geq |p|$ for the causality condition to be preserved [51,56,57].

In this section we express the reheating parameters (N_{re}, T_{re}, and w_{re}) in terms of the quantities that are derivable from inflation models [50,58–60]. Assuming a constant equation of state during reheating and using $\rho \propto a^{-3(1+w)}$, the reheating epoch can be expressed as

$$\frac{\rho_{\mathrm{end}}}{\rho_{re}} = \left(\frac{a_{\mathrm{end}}}{a_{re}}\right)^{-3(1+w_{re})}, \tag{20}$$

where the subscript "*end*" refers to the quantity evaluated at the end of inflation, and the subscript "*re*" denotes the quantity evaluated at the end of reheating. The number of e-foldings during reheating is obtained using (20) as

$$N_{re} = \ln\left(\frac{a_{re}}{a_{\mathrm{end}}}\right) = \frac{1}{3(1+w_{re})}\ln\left(\frac{\rho_{\mathrm{end}}}{\rho_{re}}\right) .= \frac{1}{3(1+w_{re})}\ln\left(\frac{3}{2}\frac{V_{\mathrm{end}}}{\rho_{re}}\right), \tag{21}$$

where we have used $\rho_{\mathrm{end}} = \frac{3}{2}V_{\mathrm{end}}$ in the last expression as $w = -\frac{1}{3}$ at the end of inflation. At the end of reheating the Universe enters into the radiation era, hence the energy density at the end of reheating can be expressed in terms of the reheating temperature as

$$\rho_{re} = \frac{\pi^2}{30} g_{re} T_{re}^4, \tag{22}$$

where g_{re} is the number of relativistic species at the end of reheating. We will use $g_{re} = 100$ (the value for standard model of particle physics) for our analysis. Using Eqs. (21) and (22) N_{re} can be expressed in terms of reheating temperature as

$$N_{re} = \frac{1}{3(1+w_{re})}\ln\left(\frac{30.\frac{3}{2}V_{\mathrm{end}}}{\pi^2 g_{re} T_{re}^4}\right). \tag{23}$$

Since the entropy remains conserved between the end of reheating and today, the reheating temperature can be related to the CMB temperature today as

$$T_{re} = T_0\left(\frac{a_0}{a_{eq}}\right)\left(\frac{43}{11 g_{re}}\right)^{1/3} = T_0\left(\frac{a_0}{a_{eq}}\right)e^{N_{RD}}\left(\frac{43}{11 g_{re}}\right)^{1/3}, \tag{24}$$

where "0" in the subscript denotes the values of the quantities evaluated at the present epoch, and "eq" refers to the values evaluated at matter-radiation equality. N_{RD} in Eq. (24) refers to the number of e-foldings during the radiation era, $e^{-N_{RD}} \equiv \frac{a_{re}}{a_{eq}}$. The ratio $\frac{a_0}{a_{eq}}$ is expressed as

$$\frac{a_0}{a_{eq}} = \frac{a_0}{a_k}\frac{a_k}{a_{\mathrm{end}}}\frac{a_{\mathrm{end}}}{a_{re}}\frac{a_{re}}{a_{eq}} = \frac{a_0 H_k}{c_S k} e^{-N_k} e^{N_{re}} e^{-N_{RD}}. \tag{25}$$

Here the subscript "k" denotes that the quantity is evaluated at the time when the Fourier mode k crosses the Hubble radius during inflation. N_k represents the number of e-folds from this time to the end of inflation, and the condition for horizon crossing $c_S k = a_k H_k$ is also used. Substituting Eq. (25) into Eq. (24), we obtain

$$T_{re} = \left(\frac{43}{11 g_{re}}\right)^{1/3} \left(\frac{a_0 T_0}{c_S k}\right) H_k e^{-N_k} e^{-N_{re}}. \tag{26}$$

Again substituting Eq. (26) into Eq. (23), one can find

$$N_{re} = \frac{4}{3(1+w_{re})}\left[\frac{1}{4}\ln\left(\frac{3^2.5}{\pi^2 g_{re}}\right) + \ln\left(\frac{V_{\rm end}^{1/4}}{H_k}\right) + \frac{1}{3}\ln\left(\frac{11 g_{re}}{43}\right) + \ln\left(\frac{c_S k}{a_0 T_0}\right) + N_k + N_{re}\right]. \tag{27}$$

This, on solving for N_{re}, with the assumption $w_{re} \neq \frac{1}{3}$, gives

$$N_{re} = \frac{4}{(1-3w_{re})}\left[\frac{-1}{4}\ln\left(\frac{3^2.5}{\pi^2 g_{re}}\right) - \frac{1}{3}\ln\left(\frac{11 g_{re}}{43}\right) - \ln\left(\frac{c_S k}{a_0 T_0}\right) - \ln\left(\frac{V_{\rm end}^{1/4}}{H_k}\right) - N_k\right]. \tag{28}$$

The reheating process is instantaneous for $w_{re} = \frac{1}{3}$ and the reheating temperature is at grand unification scale for this case. Hence the parameters of reheating can not be used for constraining models of inflation. Now we use Eq. (26) to obtain the final expression for T_{re}

$$T_{re} = \left[\left(\frac{43}{11 g_{re}}\right)^{\frac{1}{3}} \frac{a_0 T_0}{c_S k} H_k \exp^{-N_k}\left[\frac{3^2.5 V_{\rm end}}{\pi^2 g_{re}}\right]^{-\frac{1}{3(1+w_{re})}}\right]^{\frac{3(1+w_{re})}{3w_{re}-1}}. \tag{29}$$

The expressions for the number of e-folds during reheating N_{re}, (28), and the reheating temperature T_{re}, (29), are the main results of this section. It is evident that these two quantities depend on inflationary parameters H_k, N_k, and $V_{\rm end}$, which can be expressed in terms of the amplitude of scalar perturbations A_s and spectral index n_s. Hence bounds on the reheating temperature, and demanding w_{re} to lie between $-\frac{1}{3}$ and 1 provide bounds on n_s. In subsequent sections we use these reheating parameters N_{re} and T_{re} to constrain noncanonical inflation with a DBI kinetic term and the power-law kinetic term.

IV. k-INFLATION WITH A DBI KINETIC TERM

In this section we consider k-inflation with a DBI kinetic term, and monomial potentials and natural inflation potential. The Lagrangian for the scalar field in this case is given as

$$\mathcal{L} = -V(\phi)\sqrt{1-\eta^2 g^{\mu\nu}\partial_\mu\phi\partial_\nu\phi}\}. \tag{30}$$

Here η has the dimension of $[length]^2$ and the field ϕ has the dimension of mass. Using this Lagrangian we can obtain the energy density (4), and pressure (3), for the background part of the scalar field in a homogeneous and isotropic universe as

$$\rho = \frac{V(\phi)}{\sqrt{(1-\eta^2\dot{\phi}^2)}}, \tag{31}$$

$$P = -V(\phi)(1-\eta^2\dot{\phi}^2)^{\frac{1}{2}}. \tag{32}$$

Using Eq. (32) we can write the Friedmann equations for the Hubble parameter and its first derivative as

$$H^2 = \frac{1}{3M_P{}^2}\frac{V(\phi)}{(1-\eta^2\dot{\phi}^2)^{\frac{1}{2}}}, \tag{33}$$

$$\dot{H} = -\frac{V(\phi)\eta^2\dot{\phi}^2}{2M_P(1-\eta^2\dot{\phi}^2)^{\frac{1}{2}}}. \tag{34}$$

The equation of motion for the background part of the scalar field can be obtained from the energy-momentum tensor (2) as

$$\frac{\ddot{\phi}}{(1-\eta^2\dot{\phi}^2)} + 3H\dot{\phi} + \frac{V'(\phi)}{\eta^2 V(\phi)} = 0. \tag{35}$$

Here "$'$" refers to the derivative with respect to ϕ. The Hubble flow parameters ϵ_1 and ϵ_2, for k-inflation with DBI kinetic term, can be obtained by substituting the expressions for energy density and pressure (32) in Eq. (13) and Eq. (14) as

$$\epsilon_1 = \frac{3}{2}\eta^2\dot{\phi}^2, \tag{36}$$

$$\epsilon_2 = 2\frac{\ddot{\phi}}{H\dot{\phi}}. \tag{37}$$

Under the slow-roll approximation, $\ddot{\phi}$ in Eq. (35) should be smaller than the friction term $3H\dot{\phi}$, and $\eta^2\dot{\phi}^2$ can be neglected in Eq. (33). Hence we obtain

$$\dot{\phi} = -\frac{V'(\phi)}{3\eta^2 HV(\phi)}, \qquad H^2 \sim \frac{V}{3M_P^2}, \tag{38}$$

during inflation. Using these approximations, slow-roll parameters ϵ_1 and ϵ_2 can be written in terms of the inflaton potential as

$$\epsilon_1 = \frac{M_P^2}{2}\left(\frac{V'^2}{\eta^2 V^3}\right), \tag{39}$$

$$\epsilon_2 = \frac{M_P^2}{\eta^2}\left(-2\frac{V''}{V^2} + 3\frac{V'^2}{V^3}\right). \tag{40}$$

The amplitude of scalar perturbations A_S, spectral index n_s and tensor to scalar ratio can now be obtained in terms of the parameters of inflaton potential using these equations. Another parameter depending on inflaton potential is the number of e-foldings from the time when the Fourier mode k leaves the Hubble radius during inflation to the end of inflation, which can be obtained using Eq. (38) as

$$N_k = \int H dt = -\frac{\eta^2}{M_P^2}\int_{\phi_k}^{\phi_{\rm end}} \frac{V^2}{V'} d\phi. \tag{41}$$

We now impose reheating constraints on k-inflation having a DBI kinetic term with a monomial potential and PNGB potential.

A. Monomial potential

We consider the following potential

$$V(\phi) = \frac{1}{2} m^{4-n}\phi^n. \tag{42}$$

We choose $n = \frac{2}{3}$, 2, and 4 for our analysis. This potential, for canonical single-field inflation, in the context of reheating is studied in [8,50,52,56]. Using Eqs. (39) and (40) for potential (42), the slow-roll parameters can be obtained as

$$\epsilon_1 = \frac{M_P^2 n^2}{\eta^2 m^{4-n}\phi^{n+2}}, \tag{43}$$

$$\epsilon_2 = \frac{2M_P^2 n(n+2)}{\eta^2 m^{4-n}\phi^{n+2}}. \tag{44}$$

At the end of inflation $\epsilon_1 = 1$ and hence the value of the scalar field at this time can be obtained using Eq. (43) as

$$\phi_{\rm end} = \left(\frac{{M_P}^2 n^2}{\eta^2 m^{4-n}}\right)^{\frac{1}{n+2}}. \tag{45}$$

The number of e-foldings N_k for monomial potential can be obtained using Eq. (41) as

$$N_k = -\frac{\eta^2 m^{4-n}}{2M_P^2 n(n+2)}(\phi_{\rm end}^{n+2} - \phi_k^{n+2}). \tag{46}$$

Here ϕ_k is the value of the inflaton field at the time when mode k leaves the horizon during inflation. The spectral index n_s can be obtained by substituting values of ϵ_1 and ϵ_2 from Eq. (43), Eq. (44) in Eq. (17) at $\phi = \phi_k$ as

$$n_s = 1 - \frac{4M_P^2 n(n+1)}{\eta^2 m^{4-n}\phi_k^{n+2}}. \tag{47}$$

Using this equation we get

$$\phi_k = \left(\frac{4M_P^2 n(n+1)}{(1-n_s)\eta^2 m^{4-n}}\right)^{\frac{1}{n+2}}, \tag{48}$$

and the slow-roll parameter ϵ_1, (43) at $\phi = \phi_k$ is given as

$$\epsilon_1 = \frac{n^2(1-n_s)}{4n(n+1)}. \tag{49}$$

Putting the values of $\phi_{\rm end}$ and ϕ_k from Eq. (45) and Eq. (48) in Eq. (46), the number of e-foldings N_k can be expressed in terms of spectral index n_s as

$$N_k = \frac{n^2(3+n_s) + 4n}{2n(n+2)(1-n_s)}. \tag{50}$$

The inflation potential at the end of inflation will be

$$V_{\rm end} = \frac{1}{2} m^{4-n}\phi_{\rm end}^n, \tag{51}$$

which can be expressed in terms of H_k using Eq. (38) as

$$V_{\rm end} = 3M_P^2 H_k^2 \frac{\phi_{\rm end}^n}{\phi_k^n}. \tag{52}$$

Putting the values of $\phi_{\rm end}$ and ϕ_k from (45) and (48) we obtain

$$V_{\rm end} = 3M_P^2 H_k^2 \left\{\frac{n^2(1-n_s)}{4n(n+1)}\right\}^{\frac{n}{n+2}}. \tag{53}$$

The speed of sound c_S for monomial potential with a DBI kinetic term can be found using Eq. (19) as

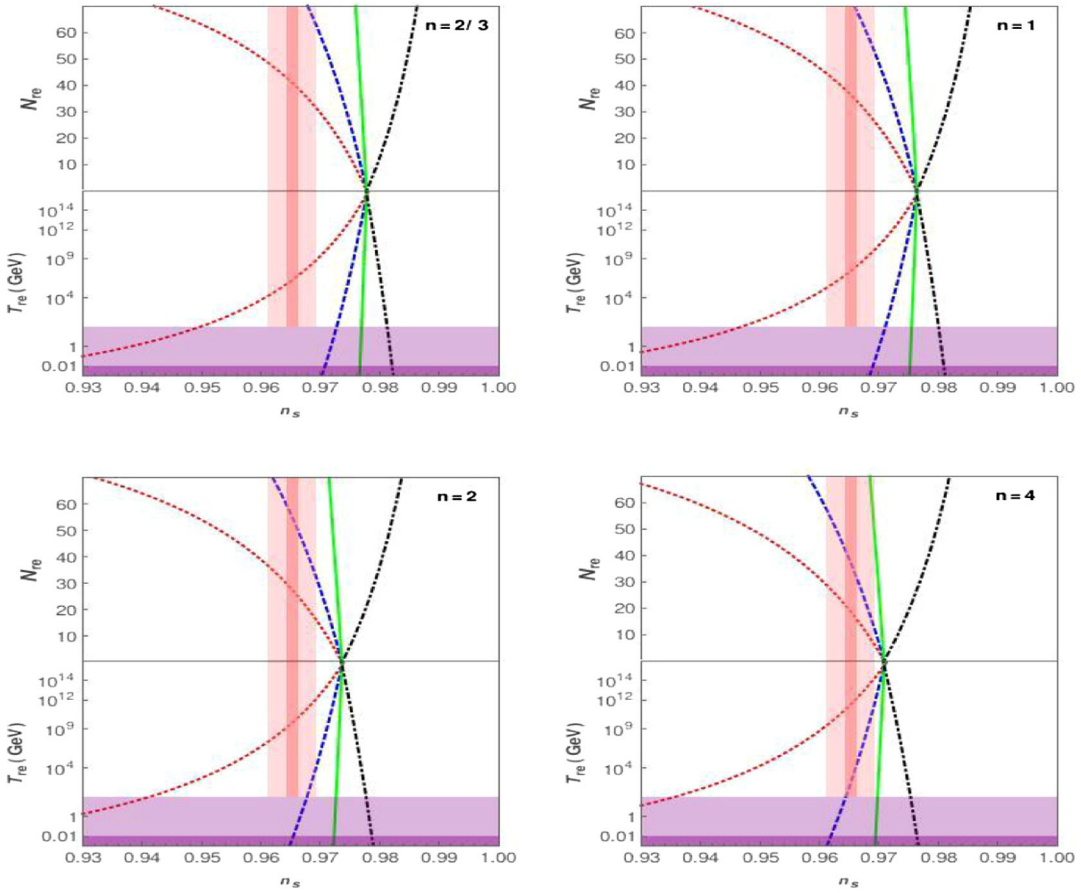

FIG. 1. N_{re} and T_{re} as function of n_s for four different values of n of monomial potential. The vertical pink region shows *Planck* 2018 bounds on n_s and the dark pink region represents a precision of 10^{-3} from future observations [61]. The horizontal purple region corresponds to T_{re} of 10 MeV from BBN and the light purple region corresponds to 100 GeV of the electroweak scale. The red dotted line corresponds to $w_{re} = -\frac{1}{3}$, the blue dashed lines corresponds to $w_{re} = 0$, the green solid line corresponds to $w_{re} = 0.25$ and the black dot-dashed line is for $w_{re} = 1$.

$$c_S = \sqrt{1 - \frac{n^2(1-n_s)}{6n(n+1)}}. \tag{54}$$

The Hubble constant H_k at the time when the mode k leaves the horizon during inflation can be expressed in terms of scalar amplitude A_S using Eq. (15) as

$$H_k = \pi M_P \sqrt{8 A_S \epsilon_1 c_S}, \tag{55}$$

which can be written in terms of spectral index n_s and A_S using Eq. (49) and Eq. (54) as

$$H_k = \pi M_P \sqrt{8 A_S \sqrt{\left\{1 - \frac{n^2(1-n_s)}{6n(n+1)}\right\}} \frac{n^2(1-n_s)}{4n(n+1)}}. \tag{56}$$

Using the expressions for N_k (50), $V_{\rm end}$ (53), and H_k (56), we can evaluate the reheating temperature T_{re} (29) and the e-folds during reheating N_{re} in terms of the spectral index for various equations of state. Figure 1 depicts the variation of the reheating temperature T_{re} and N_{re} with respect to n_s for $n = 2/3$, $n = 1$, $n = 2$, and $n = 4$. We choose four values of effective equation of states during reheating $w_{re} = -1/3$, 0, 0.25, and 1. The *Planck* 2018 bounds on $n_s = 0.9853 \pm 0.0041$ are also shown in the figure. We have used *Planck* 2018 value $A_S = 2.20 \times 10^{-9}$ for the scalar amplitude for our analysis. The point where the curves of all w_{re} meets corresponds to instant reheating, $N_{re} \to 0$. The curve for w_{re} would pass through this point and be vertical.

By demanding that the reheating temperature should be above 100 GeV for weak-scale dark matter production, we obtain bounds on spectral index by solving Eqs. (29) and (50) and assuming $-\frac{1}{3} \le w_{re} \le 1$ for various choices of n. These bounds on n_s provide bounds on the number of e-foldings N_k from Eq. (50). The tensor to scalar ratio r can be expressed in terms of n_s using Eqs. (18) and (49) as

$$r = \frac{4n^2(1-n_s)}{n(n+1)} \left[1 - \frac{n^2(1-n_s)}{6n(n+1)}\right]^{\frac{1}{2}}. \tag{57}$$

TABLE I. The allowed values of spectral index n_s and the number of e-folds N_k for various values of n for monomial potential by demanding $T_{re} \geq 100$ GeV.

n	Equation of state	n_s	N_k	r
$n = 2/3$	$-1/3 \leq w_{re} \leq 0$	$0.9497 \leq n_s \leq 0.9728$	$24.72 \leq N_k \leq 45.79$	$0.0804 \geq r \geq 0.0435$
	$0 \leq w_{re} \leq 0.25$	$0.9728 \leq n_s \leq 0.9769$	$45.79 \leq N_k \leq 54.16$	$0.0435 \geq r \geq 0.0368$
	$0.25 \leq w_{re} \leq 1$	$0.9769 \leq n_s \leq 0.9813$	$54.16 \leq N_k \leq 66.68$	$0.0368 \geq r \geq 0.0300$
$n = 1$	$-1/3 \leq w_{re} \leq 0$	$0.9468 \leq n_s \leq 0.9711$	$24.89 \leq N_k \leq 45.97$	$0.1062 \geq r \geq 0.0577$
	$0 \leq w_{re} \leq 0.25$	$0.9711 \leq n_s \leq 0.9755$	$45.97 \leq N_k \leq 54.34$	$0.0577 \geq r \geq 0.0489$
	$0.25 \leq w_{re} \leq 1$	$0.9755 \leq n_s \leq 0.9801$	$54.34 \leq N_k \leq 66.84$	$0.0489 \geq r \geq 0.0398$
$n = 2$	$-1/3 \leq w_{re} \leq 0$	$0.9411 \leq n_s \leq 0.9678$	$25.21 \leq N_k \leq 46.28$	$0.1566 \geq r \geq 0.0858$
	$0 \leq w_{re} \leq 0.25$	$0.9678 \leq n_s \leq 0.9727$	$46.28 \leq N_k \leq 54.63$	$0.0858 \geq r \geq 0.0728$
	$0.25 \leq w_{re} \leq 1$	$0.9727 \leq n_s \leq 0.9777$	$54.63 \leq N_k \leq 67.11$	$0.0728 \geq r \geq 0.0593$
$n = 4$	$-1/3 \leq w_{re} \leq 0$	$0.9355 \leq n_s \leq 0.9645$	$25.50 \leq N_k \leq 46.56$	$0.2055 \geq r \geq 0.1135$
	$0 \leq w_{re} \leq 0.25$	$0.9645 \leq n_s \leq 0.9698$	$46.56 \leq N_k \leq 54.89$	$0.1135 \geq r \geq 0.0963$
	$0.25 \leq w_{re} \leq 1$	$0.9698 \leq n_s \leq 0.9754$	$54.89 \leq N_k \leq 67.33$	$0.0963 \geq r \geq 0.0786$

Using this expression the bounds on n_s, obtained using the reheating temperature and the effective equation of state during reheating, can be transferred to the bounds on tensor to scalar ratio r.

The bounds on n_s, N_k, and r, thus obtained, are listed in Table I. It can be seen from Table I and Fig. 1 that, for $n = 2/3$ and 1, the bounds on n_s lie outside the *Planck* 2018 bounds, if we demand that the effective equation of state lies between the physically plausible range $0 \leq w_{re} \leq 0.25$. With this range of w_{re} the tensor to scalar ratio r for the quadratic and quartic potential is slightly greater than joint BICEP2/Keck Array and Planck bounds, $r < 0.06$ [62].

The plots between N_k and n_s are shown in the left panel of Fig. 2 for various values of n and w_{re}. The tensor to scalar ratio r as a function n_s for the four choices of monomial potentials, is shown in the right panel of Fig. 2 along with joint 68% and 95% C.L constraints from *Planck* 2018. It can be seen from Fig. 2 that the r vs n_s predictions for the quadratic and quartic potential with a DBI kinetic term lie within 95% C.L. but lie outside 68% C.L. of the *Planck* 2018 data for the physically plausible range of $0 \leq w_{re} \leq 0.25$. However, THE potential with $n = \frac{2}{3}$ and $n = 1$ lie well within 68% of the *Planck* 2018 observations, but, for this the equation of state during reheating should be less than 0.

B. Natural inflation potential

The potential for pseudo-Nambu-Goldstone boson, natural inflation is given as [63]

$$V(\phi) = \Lambda^4 \left[1 + \cos\left(\frac{\phi}{f}\right)\right], \tag{58}$$

where f is the spontaneous symmetry breaking scale and Λ is the explicit symmetry breaking scale for the pseudo-Nambu-Goldstone boson. Reheating constraints on this

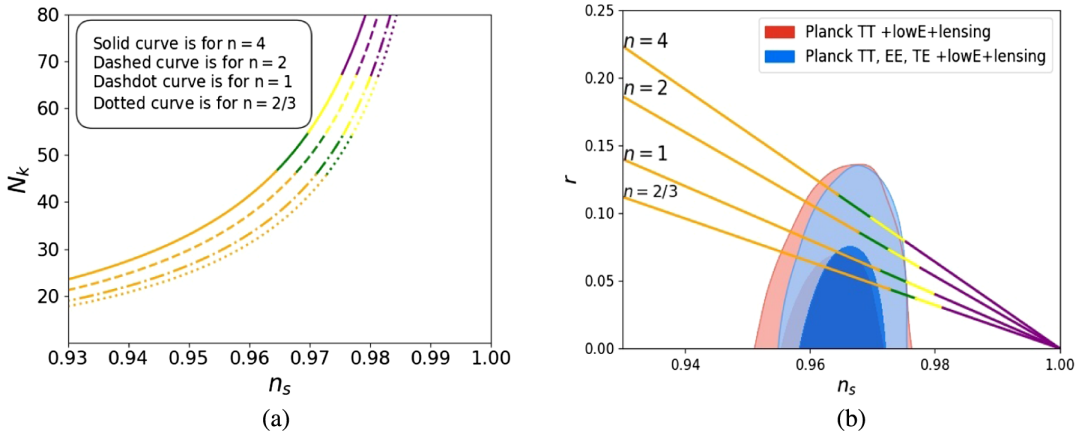

FIG. 2. N_k vs n_s, and $r - n_s$ predictions along with joint 68% C.L. and 95% C.L. *Planck* 2018 constraints for monomial potentials with DBI kinetic term. Here in both panels the orange region corresponds to $w_{re} \leq 0$, the green region corresponds to $0 \leq w_{re} \leq 0.25$, the yellow region shows $0.25 \leq w_{re} \leq 1$, and the purple region corresponds to $w_{re} > 1$. (a) N_k vs n_s plot for $n = \frac{2}{3}, 1, 2, 4$. (b) r vs n_s plot for $n = \frac{2}{3}, 1, 2, 4$.

potential with noncanonical kinetic term having DBI form are discussed in [24]. Here we revisit these constraints with *Planck* 2018 data. Defining $\beta \equiv \eta^2 f^2 \Lambda^4 M_P^{-2}$, the slow-roll parameters for the potential given in Eq. (58) can be obtained using Eqs. (39) and (40) as

$$\epsilon_1 = \frac{1}{2\beta}\frac{1-\cos(\frac{\phi}{f})}{\{1+\cos(\frac{\phi}{f})\}^2}, \tag{59}$$

$$\epsilon_2 = \frac{1}{\beta}\frac{3-\cos(\frac{\phi}{f})}{\{1+\cos(\frac{\phi}{f})\}^2}. \tag{60}$$

The value of the inflaton field at the end of inflation can be obtained by setting $\epsilon_1 = 1$ as

$$\cos\left(\frac{\phi_{\rm end}}{f}\right) = \frac{-(4\beta+1)+\sqrt{(1+16\beta)}}{4\beta}. \tag{61}$$

The spectral index n_s can be obtained by substituting values of ϵ_1 (59) and ϵ_2 (60) in Eq. (17) as

$$n_s = 1 - \frac{1}{\beta}\frac{1-\cos(\frac{\phi}{f})}{\{1+\cos(\frac{\phi}{f})\}^2} - \frac{1}{\beta}\frac{3-\cos(\frac{\phi}{f})}{\{1+\cos(\frac{\phi}{f})\}^2} \tag{62}$$

$$= 1 - \frac{2[2-\cos(\frac{\phi}{f})]}{\beta[1+\cos(\frac{\phi}{f})]^2}. \tag{63}$$

The number of e-foldings for potential (58) can be expressed using Eq. (41) and as for natural inflation potential Eq. (58), N_k can be written as

$$N_k = \frac{\beta}{f}\int_{\phi_k}^{\phi_{\rm end}} \frac{[1+\cos(\frac{\phi}{f})]^2}{\sin(\frac{\phi}{f})}$$

$$= \beta\left[\cos\left(\frac{\phi_{\rm end}}{f}\right) - \cos\left(\frac{\phi_k}{f}\right)\right] + 2\beta\ln\left[\frac{\cos(.\frac{\phi_{\rm end}}{f})-1}{\cos(\frac{\phi_k}{f})-1}\right], \tag{64}$$

where again $\phi_{\rm end}$ and ϕ_k are the values of the inflaton field at the end of inflation and at the time the mode k leaves inflationary horizon during inflation, respectively. Defining $\cos(\frac{\phi_{\rm end}}{f}) = x$ and $\cos(\frac{\phi_k}{f}) = y$, Eq. (64) for the number of e-folds N_k can be written as

$$N_k = \beta x - \beta y + 2\beta\ln(x-1) - 2\beta\ln(y-1). \tag{65}$$

The spectral index n_s, (63), at $\phi = \phi_k$ will have the form in terms of y as

$$n_s = 1 - \frac{2}{\beta}\frac{(2-y)}{(1+y)^2}. \tag{66}$$

To express N_k in terms of n_s, Eq. (66) can be solved for y as

$$y = 1 + \frac{1+2\beta-2n_s\beta-\sqrt{1+6\beta-6n_s\beta}}{n_s\beta-\beta}, \tag{67}$$

and x is given by Eq. (61). The inflaton potential at the end of inflation can be given as

$$V_{\rm end} = \Lambda^4\left[1+\cos\left(\frac{\phi_{\rm end}}{f}\right)\right], \tag{68}$$

which can be written using Eq. (38) as

$$V_{\rm end} = 3M_P^2H_k^2\frac{[1+\cos(\frac{\phi_{\rm end}}{f})]}{[1+\cos(\frac{\phi_k}{f})]}$$

$$= 3M_P^2H_k^2\frac{(1+x)}{(1+y)}. \tag{69}$$

From Eq. (19), the speed of sound c_S at $\phi = \phi_k$ can be written as

$$c_S = \sqrt{1-\frac{1}{3\beta}\frac{(1-\cos(\frac{\phi_k}{f}))}{(1+\cos(\frac{\phi_k}{f}))^2}},$$

$$= \sqrt{1-\frac{1}{3\beta}\frac{(1-y)}{(1+y)^2}}. \tag{70}$$

The value of the Hubble constant at the time when Fourier mode k leaves the inflationary horizon during inflation can again be expressed in terms of amplitude of scalar perturbations A_S by putting the values of ϵ_1 (59), and c_S, (70), in Eq. (15) as

$$H_k = \pi M_P\sqrt{8A_S\frac{1}{2\beta}\frac{1-y}{(1+y)^2}\sqrt{1-\frac{1}{3\beta}\frac{(1-y)}{(1+y)^2}}}. \tag{71}$$

We can express N_k, $V_{\rm end}$, and H_k in terms of spectral index by substituting the value of y from Eq. (67) and x from Eq. (61) in Eq. (65), Eq. (69), and Eq. (71), and then using these expressions the reheating temperature T_{re} and the number of e-folds during reheating N_{re} can be obtained in terms of the spectral index from Eqs. (28) and (29). We have chosen $\beta = 35$, 50, 100, and 125 for our analysis. Increasing β beyond 125 does not affect the results. The variation of N_{re} and T_{re} with respect to n_s, along with *Planck* 2018 bounds on $n_s = 0.9853 \pm 0.0041$, is represented in Fig. 3 for various values of effective equation of state during reheating. Again the curves for various values of w_{re} meet at the point corresponding to instant reheating, $N_{re} \to 0$. The curve for $w_{re} = 1/3$ would pass through this point and be vertical.

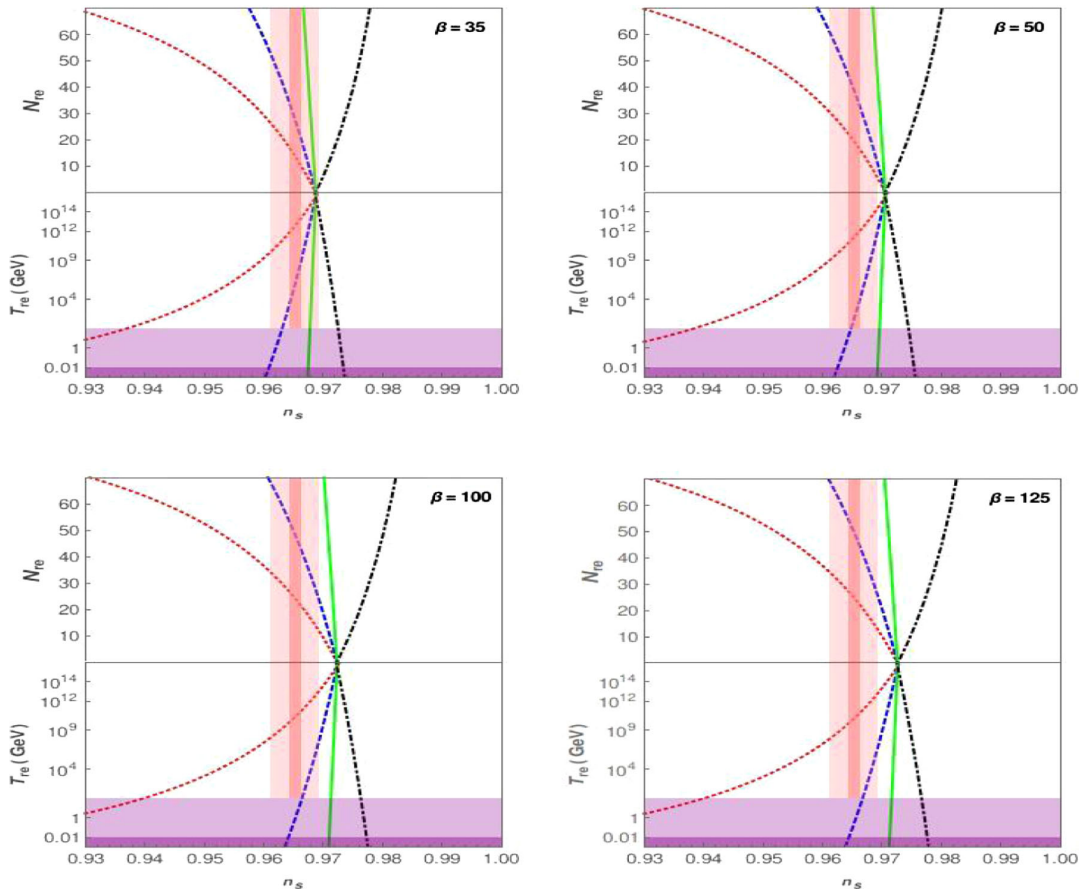

FIG. 3. N_{re} and T_{re} as function of n_s for natural inflation potential. The vertical pink region shows *Planck* 2018 bounds on n_s and the dark pink region represents a precision of 10^{-3} from future observations [61]. The horizontal purple region corresponds to T_{re} of 10 MeV from BBN and the light purple region corresponds to 100 GeV of the electroweak scale. The red dotted line corresponds to $w_{re} = -\frac{1}{3}$, the blue dashed line corresponds to $w_{re} = 0$, the green solid line corresponds to $w_{re} = 0.25$ and the black dot-dashed line is for $w_{re} = 1$.

By imposing the bounds on T_{re}, i.e., $T_{re} > 100$ GeV for weak-scale dark matter production, we obtain bounds on n_s for various equation of states w_{re} by solving Eq. (29). Again the tensor to scalar ratio for natural inflation with a DBI kinetic term can be obtained from Eqs. (16), (59), (70) as

TABLE II. The allowed values of spectral index n_s and number of e-folds N_k for various values of β for natural inflation potential, obtained by imposing $T_{re} \geq 100$ GeV.

α	Equation of state	n_s	N_k	r
$\beta = 35$	$-1/3 \leq w_{re} \leq 0$	$0.9369 \leq n_s \leq 0.9631$	$25.08 \leq N_k \leq 46.06$	$0.1072 \geq r \geq 0.0480$
	$0 \leq w_{re} \leq 0.25$	$0.9631 \leq n_s \leq 0.9678$	$46.06 \leq N_k \leq 54.37$	$0.0480 \geq r \geq 0.0377$
	$0.25 \leq w_{re} \leq 1$	$0.9678 \leq n_s \leq 0.9725$	$54.37 \leq N_k \leq 66.78$	$0.0377 \geq r \geq 0.0274$
$\beta = 50$	$-1/3 \leq w_{re} \leq 0$	$0.9384 \leq n_s \leq 0.9648$	$25.10 \leq N_k \leq 46.10$	$0.1159 \geq r \geq 0.0547$
	$0 \leq w_{re} \leq 0.25$	$0.9648 \leq n_s \leq 0.9696$	$46.10 \leq N_k \leq 54.42$	$0.0547 \geq r \geq 0.0438$
	$0.25 \leq w_{re} \leq 1$	$0.9696 \leq n_s \leq 0.9745$	$54.42 \leq N_k \leq 66.86$	$0.0438 \geq r \geq 0.0329$
$\beta = 100$	$-1/3 \leq w_{re} \leq 0$	$0.9398 \leq n_s \leq 0.9665$	$25.13 \leq N_k \leq 46.16$	$0.1287 \geq r \geq 0.0645$
	$0 \leq w_{re} \leq 0.25$	$0.9665 \leq n_s \leq 0.9713$	$46.16 \leq N_k \leq 54.49$	$0.0645 \geq r \geq 0.0529$
	$0.25 \leq w_{re} \leq 1$	$0.9713 \leq n_s \leq 0.9764$	$54.49 \leq N_k \leq 66.95$	$0.0529 \geq r \geq 0.0412$
$\beta = 125$	$-1/3 \leq w_{re} \leq 0$	$0.9401 \leq n_s \leq 0.9668$	$25.14 \leq N_k \leq 46.18$	$0.1318 \geq r \geq 0.0669$
	$0 \leq w_{re} \leq 0.25$	$0.9668 \leq n_s \leq 0.9717$	$46.18 \leq N_k \leq 54.51$	$0.0669 \geq r \geq 0.0552$
	$0.25 \leq w_{re} \leq 1$	$0.9717 \leq n_s \leq 0.9767$	$54.51 \leq N_k \leq 66.97$	$0.0552 \geq r \geq 0.0432$

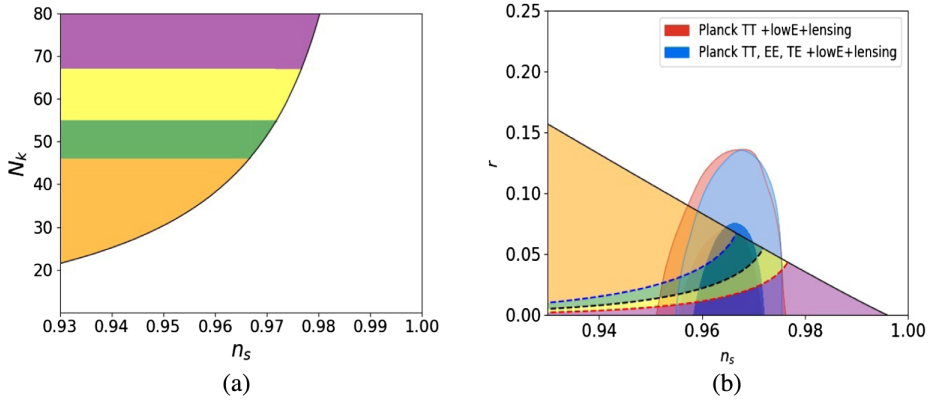

FIG. 4. N_k vs n_s and r vs n_s plots for natural inflation potential along with joint 68% C.L. and 95% C.L. *Planck* 2018 constraints. In both the panels the orange region corresponds to $w_{re} < 0$, the green region corresponds to $0 < w_{re} < 0.25$, the yellow region corresponds to $0.25 < w_{re} < 1$, and the purple region corresponds to $w_{re} > 1$. In the right panel of the figure the blue dashed line corresponds to $N_k = 46$, the black dashed line corresponds to $N_k = 55$ and the red dashed line corresponds to $N_k = 67$. These values of N_k correspond to bounds on n_s obtained by demanding $T_{re} > 100$ GeV for different values of w_{re}. The solid black line in both the panels of the figure corresponds to $\beta = 125$ and the filled region corresponds to $\beta < 125$. (a) N_k vs n_s plot for $\beta < 125$. (b) r vs $n_s$plot for $\beta < 125$.

$$r = \frac{8}{2\beta}\frac{(1-y)}{(1+y)^2}\sqrt{1-\frac{1}{3\beta}\frac{(1-y)}{(1+y)^2}}. \tag{72}$$

The bounds on n_s obtained from T_{re} and w_{re} can give bounds on N_k and r. These bounds for various choices of β are given in Table II

It can be seen from Table II that with the physically plausible range $0 \leq w_{re} \leq 0.25$ the bounds on n_s and r are compatible with *Planck* 2018 observations for $\beta < 125$. We also show N_k vs n_s and r vs n_s plots for the PNGB potential with a DBI kinetic term in Fig. 4. It is evident from the figure that the values of n_s and r predicted in this model lie within 1σ contour of *Planck* 2018 joint constraints for physically plausible range $0 \leq w_{re} \leq 0.25$ shown by green region in the figure. Our results for natural inflation with a DBI kinetic term agree with [24].

V. k-INFLATION WITH A POWER-LAW KINETIC TERM

In this section we will analyze k-inflation with a power-law kinetic term. The Lagrangian density for this case is given as [11,23]

$$L(X,\phi) = X\left(\frac{X}{M^4}\right)^{\alpha-1} - V(\phi), \tag{73}$$

where M has dimension of mass and α is dimensionless. For $\alpha = 1$ the Lagrangian reduces to usual canonical scalar field. Using Eqs. (4) and (3) the energy density and pressure can be obtained as

$$\rho_\phi = (2\alpha-1)X\left(\frac{X}{M}\right)^{\alpha-1} + V(\phi), \tag{74}$$

$$p_\phi = X\left(\frac{X}{M}\right)^{\alpha-1} - V(\phi), \qquad X \equiv \frac{1}{2}\dot{\phi}^2. \tag{75}$$

Thus, the Friedman equations for Hubble constant and its first derivative become

$$H^2 = \frac{8\pi G}{3}\left[(2\alpha-1)X\left(\frac{X}{M^4}\right)^{\alpha-1} + V(\phi)\right], \tag{76}$$

$$\dot{H} = -4\pi G(\rho_\phi + p_\phi) = -\frac{1}{3M_P^2}X\left(\frac{X}{M^4}\right)^{\alpha-1}. \tag{77}$$

The evolution equation for inflaton ϕ can be obtained by the energy-momentum tensor (2) as

$$\ddot{\phi} + \frac{3H\dot{\phi}}{2\alpha-1} + \left(\frac{V'(\phi)}{\alpha(2\alpha-1)}\right)\left(\frac{2M^4}{\dot{\phi}^2}\right)^{\alpha-1} = 0. \tag{78}$$

Using the definition of the slow-roll parameter $\epsilon = -\dot{H}/H^2$, along with Eq. (77), the Hubble constant (76) can be written as

$$H^2\left[1 - \left(\frac{2\alpha-1}{3\alpha}\right)\epsilon\right] = \frac{1}{3M_P^2}V(\phi), \tag{79}$$

under slow-roll approximation $\epsilon \ll 1$ this reduces to

$$H^2 = \frac{V(\phi)}{3M_P^2}. \tag{80}$$

For slow-roll $\ddot{\phi}$ is much smaller than the friction term in Eq. (78), hence using Eq. (80), we obtain

$$\dot{\phi} = \left[\left(\frac{M_P}{\alpha\sqrt{3}}\right)\left(\frac{-V'(\phi)}{\sqrt{V}}\right)(2M^4)^{\alpha-1}\right]^{\frac{1}{2\alpha-1}}. \quad (81)$$

The two Hubble flow parameters ϵ_1 (13), and ϵ_2 (14), for this case can be obtained using Eqs. (74), (75), (80), and Eq. (81), as

$$\epsilon_1 = \left[\frac{1}{\alpha}\left(\frac{3M^4}{V}\right)^{\alpha-1}\left(\frac{-M_P V'}{\sqrt{2}V}\right)^{2\alpha}\right]^{\frac{1}{2\alpha-1}}, \quad (82)$$

$$\epsilon_2 = \frac{-2\epsilon_1}{2\alpha-1}\left[2\alpha\left(\frac{V''V}{V'^2}\right) - (3\alpha-1)\right]. \quad (83)$$

Now the number of e-foldings N_k from the time when mode k leaves the horizon to the end of inflation, in case of power-law kinetic term, can be obtained by using

$$N_k = -\int_{\phi_{\rm end}}^{\phi_k}\left(\frac{H}{\dot{\phi}}\right)d\phi, \quad (84)$$

and substituting the values of H and $\dot{\phi}$ from Eqs. (80) and (81) respectively in this expression for various choices of potentials. The speed of sound c_S, defined in Eq. (19), can be obtained using Eq. (74) and Eq. (75) as

$$c_S^2 = \frac{1}{2\alpha-1}. \quad (85)$$

The speed of sound here is only function of α and is independent of choice of potential.

A. Monomial potentials

We consider the following monomial potential with power-law kinetic term

$$V(\phi) = \frac{1}{2}m^{4-n}\phi^n, \quad \text{where } n > 0. \quad (86)$$

The two Hubble-flow parameters for this potential can be obtained using Eqs. (82) and (83)

$$\epsilon_1 = \left[\frac{1}{\alpha}\left(\frac{6M^4}{m^{4-n}}\right)^{(\alpha-1)}\left(\frac{-nM_P}{\sqrt{2}}\right)^{2\alpha}\frac{1}{\phi^{2\alpha+n\alpha-n}}\right]^{\frac{1}{2\alpha-1}}, \quad (87)$$

$$\epsilon_2 = \frac{2\epsilon_1\gamma}{n}. \quad (88)$$

Here

$$\gamma \equiv \frac{2\alpha + n(\alpha-1)}{2\alpha-1}. \quad (89)$$

The value of the inflaton field at the end of inflation, $\phi_{\rm end}$, can be obtained by setting $\epsilon_1 = 1$ as

$$\phi_{\rm end} = \left[\frac{1}{\alpha}\left(\frac{6M^4}{m^{4-n}}\right)^{(\alpha-1)}\left(\frac{-nM_P}{\sqrt{2}}\right)^{2\alpha}\right]^{\frac{1}{\gamma(2\alpha-1)}}. \quad (90)$$

We can obtain the values of H and $\dot{\phi}$ from Eqs. (80) and (81) respectively for the monomial potential (86) and substitute these values into Eq. (84) to obtain the number of e-foldings N_k as

$$N_k = \frac{\phi_k^\gamma - \phi_{\rm end}^\gamma}{\gamma}\left[\left(\frac{m^{4-n}}{12M^4}\right)^{\alpha-1}\frac{\alpha}{nM_p^{2\alpha}}(-1)^{2(\alpha-1)}\right]^{\frac{1}{2\alpha-1}}. \quad (91)$$

With $\phi_{\rm end}$ from Eq. (90), we can obtain the expression for the inflaton field ϕ_k when the mode k leaves the horizon as

$$\phi_k = C_1^{1/\gamma}\left(N_k\gamma + \frac{n}{2}\right)^{\frac{1}{\gamma}}, \quad (92)$$

where

$$C_1 = \left\{\left(\frac{n(-M_P)^{2\alpha}}{\alpha}\right)\left(\frac{12M^4}{m^{4-n}}\right)^{\alpha-1}\right\}^{\frac{1}{2\alpha-1}}. \quad (93)$$

The first slow-roll parameter ϵ_1 can be expressed as a function of N_k by substituting Eq. (92) in Eq. (87) as

$$\epsilon_1 = \frac{n}{2N_k\gamma + n}. \quad (94)$$

Putting values of ϵ_1 and ϵ_2 from Eq. (94) and Eq. (88) in the definition of the scalar spectral index n_s (17), we obtain

$$n_s = 1 - 2\frac{(n+\gamma)}{2N_k\gamma + n}, \quad (95)$$

which, on solving for the e-folds N_k becomes

$$N_k = \frac{1}{2\gamma}\left(\frac{2(\gamma+n)}{1-n_s} - n\right). \quad (96)$$

Using Eq. (80) and Eq. (86), the value of the potential at the end of inflation can be obtained as

$$V_{\rm end} = 3M_P^2H_k^2\left(\frac{\phi_{\rm end}}{\phi_k}\right)^n. \quad (97)$$

Substituting Eq. (90) and Eq. (92) in Eq. (97) we get

$$V_{\rm end} = 3M_P^2H_k^2\left(\frac{n}{2N_k\gamma + n}\right)^{\frac{n}{\gamma}}. \quad (98)$$

By substituting the value of c_S from Eq. (85) and ϵ_1 from Eq. (94) in Eq. (15), we can express the Hubble constant H_K (at the time when the Fourier mode k leaves the inflationary horizon) as

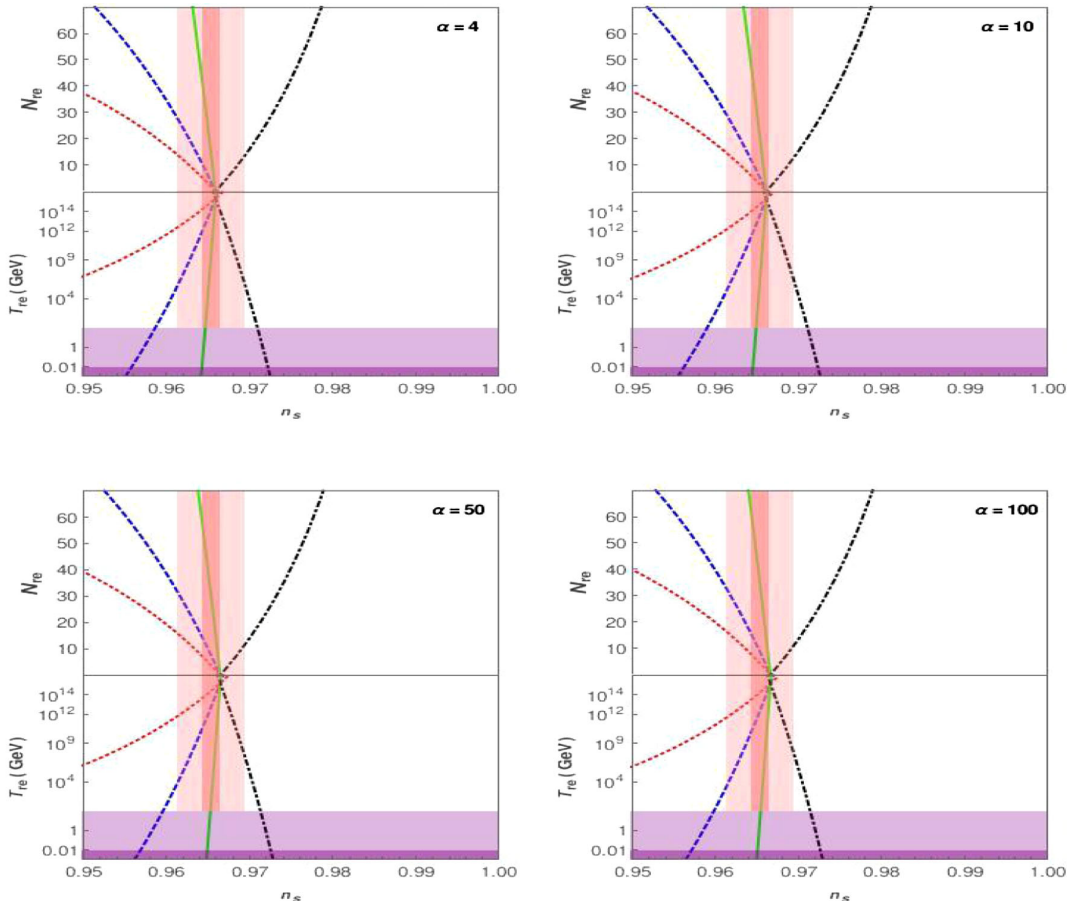

FIG. 5. N_{re} and T_{re} as a function of n_s for four different values of α of quadratic potential with a power-law kinetic term. The vertical pink region shows *Planck* 2018 bounds on n_s and the dark pink region represents a precision of 10^{-3} from future observations [61]. The horizontal purple region corresponds to T_{re} of 10 MeV from BBN and the light purple region corresponds to 100 GeV of the electroweak scale. The red dotted line corresponds to $w_{re} = -\frac{1}{3}$, the blue dashed line corresponds to $w_{re} = 0$, the green solid line corresponds to $w_{re} = 0.25$, and the black dot-dashed line is for $w_{re} = 1$.

$$H_k = \pi M_P \sqrt{8A_S \left(\frac{n}{2N_k\gamma + n}\right)\left(\frac{1}{\sqrt{2\alpha - 1}}\right)}. \quad (99)$$

Using Eq. (96) we can express Eq. (98) and Eq. (99) for $V_{\rm end}$ and H_K respectively in terms of n_s. Further, these expressions can be used to obtain the reheating temperature T_{re}, given by (29), and the number of e-folds during reheating N_{re}, given by (28), as a function of the spectral index n_s.

Here we choose quadratic $n = 2$ and quartic $n = 4$ potentials for our analysis. The variation of N_{re} and T_{re} as a function of n_s, for various values of effective equation of states, is depicted in Fig. 5 and Fig. 6 for quadratic and quartic potentials respectively along with *Planck* 2018 bounds $n_s = 0.9853 \pm 0.0041$. It is evident from Fig. 5 and Fig. 6 that, for both of these potentials, the variation of T_{re} and N_{re} with respect to n_s is independent of the power of the kinetic term α. Again we imposing the bounds on T_{re}, i.e., $T_{re} > 100$ GeV to obtain bounds on n_s for various equation of states w_{re} by solving Eq. (29). Now the tensor to scalar ratio r, (18), for the monomial potential with a power-law kinetic term can be obtained using the expressions for c_S, (85) and ϵ_1 (94), as

$$r = \left(\frac{1}{\sqrt{2\alpha - 1}}\right)\left(\frac{16n}{2N_k\gamma + n}\right). \quad (100)$$

Using the bounds on n_s, obtained from the reheating consideration, we get the bounds on N_k and the tensor to scalar ratio r for various w_{re} from Eqs. (96) and (100). These bounds on n_s, N_k, and r, thus obtained, for quadratic and quartic potentials with a power-law kinetic term are provided in Table III and Table IV. The bounds on n_s obtained from reheating are independent of α for quadratic potentials. However, the bounds obtained on tensor to scalar ratio r depend on α for both the potentials. It can be seen from Table IV that, with $\alpha = 4$, the bounds on the tensor to scalar ratio $0.086 \geq r \geq 0.0740$ lie slightly higher than the joint BICEP2/Keck array and *Planck* 2018 bound

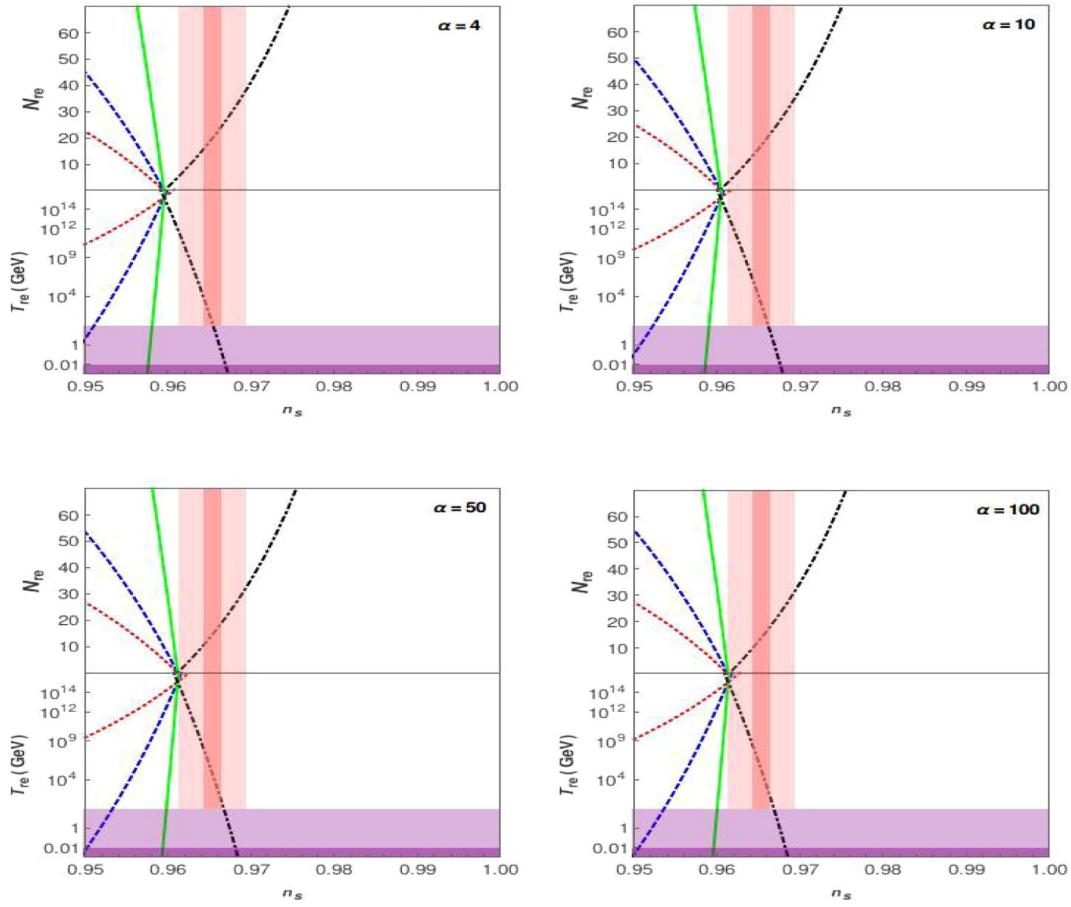

FIG. 6. N_{re} and T_{re} as function of n_s for four different values of α of quartic potential with a power-law kinetic term. The vertical pink region shows *Planck* 2018 bounds on n_s and the dark pink region represents a precision of 10^{-3} from future observations [61]. The horizontal purple region corresponds to T_{re} of 10 MeV from BBN and light purple region corresponds to 100 GeV of the electroweak scale. The red dotted line corresponds to $w_{re} = -\frac{1}{3}$, the blue dashed lines corresponds to $w_{re} = 0$, the green solid line corresponds to $w_{re} = 0.25$, and the black dot-dashed line is for $w_{re} = 1$.

TABLE III. The allowed values of spectral index n_s and number of e-folds N_k for various values of α for quadratic potential with power-law kinetic term considering $T_{re} \geq 100$ GeV.

α	Equation of state	n_s	N_k	r
$\alpha = 4$	$-1/3 \leq w_{re} \leq 0$	$0.9273 \leq n_s \leq 0.9586$	$27.02 \leq N_k \leq 47.85$	$0.1098 \geq r \geq 0.0625$
	$0 \leq w_{re} \leq 0.25$	$0.9586 \leq n_s \leq 0.9640$	$47.85 \leq N_k \leq 56.07$	$0.0625 \geq r \geq 0.0534$
	$0.25 \leq w_{re} \leq 1$	$0.9640 \leq n_s \leq 0.9709$	$56.07 \leq N_k \leq 68.33$	$0.0534 \geq r \geq 0.0439$
$\alpha = 10$	$-1/3 \leq w_{re} \leq 0$	$0.9287 \leq n_s \leq 0.9589$	$27.53 \leq N_k \leq 48.27$	$0.0655 \geq r \geq 0.0376$
	$0 \leq w_{re} \leq 0.25$	$0.9589 \leq n_s \leq 0.9649$	$48.27 \leq N_k \leq 56.45$	$0.0376 \geq r \geq 0.0322$
	$0.25 \leq w_{re} \leq 1$	$0.9649 \leq n_s \leq 0.9710$	$56.45 \leq N_k \leq 68.67$	$0.0322 \geq r \geq 0.0265$
$\alpha = 50$	$-1/3 \leq w_{re} \leq 0$	$0.9307 \leq n_s \leq 0.9596$	$28.38 \leq N_k \leq 48.96$	$0.0278 \geq r \geq 0.0163$
	$0 \leq w_{re} \leq 0.25$	$0.9596 \leq n_s \leq 0.9653$	$48.96 \leq N_k \leq 57.09$	$0.0163 \geq r \geq 0.0140$
	$0.25 \leq w_{re} \leq 1$	$0.9653 \leq n_s \leq 0.9713$	$57.09 \leq N_k \leq 69.22$	$0.0140 \geq r \geq 0.0115$
$\alpha = 100$	$-1/3 \leq w_{re} \leq 0$	$0.9315 \leq n_s \leq 0.9598$	$28.73 \leq N_k \leq 49.25$	$0.0194 \geq r \geq 0.0114$
	$0 \leq w_{re} \leq 0.25$	$0.9598 \leq n_s \leq 0.9654$	$49.25 \leq N_k \leq 57.36$	$0.0114 \geq r \geq 0.0098$
	$0.25 \leq w_{re} \leq 1$	$0.9654 \leq n_s \leq 0.9714$	$57.36 \leq N_k \leq 69.45$	$0.0098 \geq r \geq 0.0081$

TABLE IV. The allowed values of spectral index n_s and number of e-folds N_k for various values of α for the quartic potential with a power-law kinetic term considering $T_{re} \geq 100$ GeV.

α	Equation of state	n_s	N_k	r
$\alpha = 4$	$-1/3 \leq w_{re} \leq 0$	$0.9152 \leq n_s \leq 0.9510$	$27.62 \leq N_k \leq 48.36$	$0.1495 \geq r \geq 0.0863$
	$0 \leq w_{re} \leq 0.25$	$0.9510 \leq n_s \leq 0.9581$	$48.36 \leq N_k \leq 56.53$	$0.0863 \geq r \geq 0.0740$
	$0.25 \leq w_{re} \leq 1$	$0.9581 \leq n_s \leq 0.9654$	$56.53 \leq N_k \leq 68.69$	$0.0740 \geq r \geq 0.0610$
$\alpha = 10$	$-1/3 \leq w_{re} \leq 0$	$0.9180 \leq n_s \leq 0.9522$	$28.06 \leq N_k \leq 48.73$	$0.0867 \geq r \geq 0.0505$
	$0 \leq w_{re} \leq 0.25$	$0.9522 \leq n_s \leq 0.9590$	$48.73 \leq N_k \leq 56.87$	$0.0505 \geq r \geq 0.0433$
	$0.25 \leq w_{re} \leq 1$	$0.9590 \leq n_s \leq 0.9662$	$56.87 \leq N_k \leq 68.99$	$0.0433 \geq r \geq 0.0357$
$\alpha = 50$	$-1/3 \leq w_{re} \leq 0$	$0.9209 \leq n_s \leq 0.9533$	$28.88 \leq N_k \leq 49.10$	$0.0364 \geq r \geq 0.0215$
	$0 \leq w_{re} \leq 0.25$	$0.9533 \leq n_s \leq 0.9598$	$49.10 \leq N_k \leq 57.48$	$0.0215 \geq r \geq 0.0185$
	$0.25 \leq w_{re} \leq 1$	$0.9598 \leq n_s \leq 0.9667$	$57.48 \leq N_k \leq 69.52$	$0.0185 \geq r \geq 0.0153$
$\alpha = 100$	$-1/3 \leq w_{re} \leq 0$	$0.9219 \leq n_s \leq 0.9536$	$29.23 \leq N_k \leq 49.69$	$0.0253 \geq r \geq 0.0150$
	$0 \leq w_{re} \leq 0.25$	$0.9536 \leq n_s \leq 0.9600$	$49.69 \leq N_k \leq 57.75$	$0.0150 \geq r \geq 0.0129$
	$0.25 \leq w_{re} \leq 1$	$0.9600 \leq n_s \leq 0.9668$	$57.75 \leq N_k \leq 69.76$	$0.0129 \geq r \geq 0.0108$

$r < 0.06$ [62] for the physically plausible range $0 \leq w_{re} \leq 0.25$ for effective equation of states during reheating. But, for larger values of α the bounds on r are in agreement with BICEP2/Keck array bound.

Plots for N_k vs n_s for quadratic and quartic potentials are shown in Fig. 7. Here we have chosen only one value ($\alpha = 4$) for the quadratic potential, as the variation of N_k with respect to n_s is independent of α. In case of the quartic potential we have also chosen only the smallest and largest values of α, because the variation of functional dependence of N_k on n_s with respect to α is very small. Figure 8 depicts the r vs n_s predictions for quadratic and quartic potentials for different values of α and w_{re}, along with joint 68% C.L. and 95% C.L. constraints from *Planck* 2018. It can be seen from Fig. 8 that r vs n_s predictions for the quadratic potential with a power-law kinetic term lie within 68% C.L. of *Planck* 2018 constraints for the physically plausible range of $0 \leq w_{re} \leq 0.25$. However, for the quartic potential the equation of state during reheating should be greater than 0.25 for $r - n_s$ predictions to lie within 68% C.L. of *Planck* 2018 constraints.

B. Exponential potential

We now consider the exponential potential with power-law kinetic term. This potential have the following form

$$V(\phi) = V_0 \exp\left(-\sqrt{\frac{2}{q}}\frac{\phi}{M_P}\right). \tag{101}$$

In case of inflation with a canonical scalar field this potential provides a power-law expansion, $a(t) \propto t^q$, for a flat universe [64–66]. The power-law solutions can also be obtained with this potential in DBI framework [67].

We can obtain the slow-roll parameters ϵ_1 and ϵ_2 for this potential using Eq. (82) and Eq. (83) as

$$\epsilon_1 = \left[\frac{1}{\alpha}\left(\frac{3M^4}{V_0}\right)^{\alpha-1}\left(\frac{1}{\sqrt{q}}\right)^{2\alpha}\frac{1}{\exp\left(-\sqrt{\frac{2}{q}}\frac{\phi(\alpha-1)}{M_P}\right)}\right]^{\frac{1}{2\alpha-1}}, \tag{102}$$

$$\epsilon_2 = 2\epsilon_1\left(\frac{\alpha-1}{2\alpha-1}\right). \tag{103}$$

Now we evaluate $\phi_{\rm end}$, the value of inflaton field at the end of inflation, by setting $\epsilon_1 = 1$ as

$$\phi_{\rm end} = -\frac{M_P}{\alpha-1}\sqrt{\frac{q}{2}}\ln\left[\frac{1}{\alpha}\left(\frac{3M^4}{V_0}\right)^{\alpha-1}\left(\sqrt{\frac{1}{q}}\right)^{2\alpha}\right]. \tag{104}$$

To obtain the number of e-foldings N_k from the time when the Fourier mode k leaves the Hubble radius to the end of inflation, for (101), we put values of H and $\dot{\phi}$ from Eqs. (80) and (81) into Eq. (84), and on integrating it we get

$$N_k = \frac{\phi_k^{\frac{\alpha-1}{2\alpha-1}} - \phi_{\rm end}^{\frac{\alpha-1}{2\alpha-1}}}{2^{\frac{\alpha-1}{2\alpha-1}}}\left(\frac{V_0}{3M^4}\right)^{\frac{\alpha-1}{2\alpha-1}}\left(\sqrt{\frac{q}{2}}\right)^{\frac{2\alpha}{2\alpha-1}}\alpha^{\frac{1}{2\alpha-1}}. \tag{105}$$

Substituting $\phi_{\rm end}$ from Eq. (104) and solving for ϕ_k, the value of the inflaton field at the horizon crossing, we obtain

$$\phi_k = -\sqrt{\frac{q}{2}}\frac{M_P}{(\alpha-1)}\ln\left[\frac{1}{\alpha}\left(\frac{3M^4}{V_0}\right)^{\alpha-1}\left(\sqrt{\frac{2}{q}}\right)^{2\alpha}\left(\frac{1}{2^{\frac{\alpha}{2\alpha-1}}} + N_k\left(\frac{\alpha-1}{2\alpha-1}\right)2^{\frac{\alpha-1}{2\alpha-1}}\right)^{2\alpha-1}\right]. \tag{106}$$

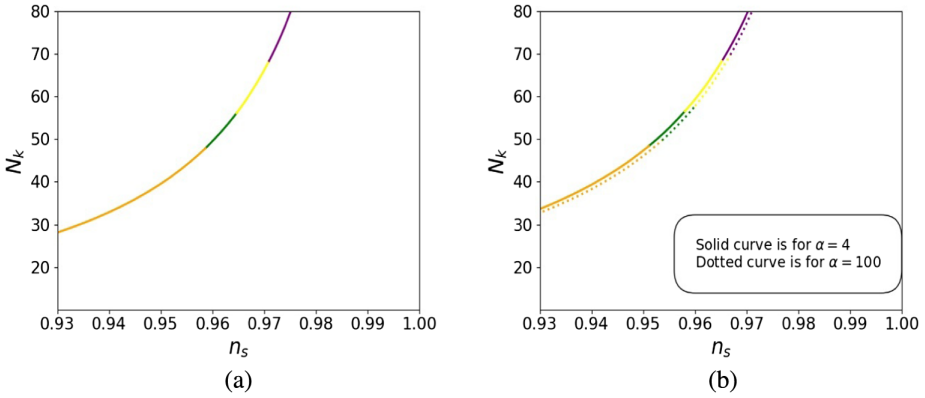

FIG. 7. N_k as function of n_s for quadratic potential and quartic potential with a power law kinetic term. N_k vs n_s for quadratic potential (b) N_k vs n_s for quartic potential.

Substituting Eq. (106) in Eq. (102), we can evaluate the first slow-roll parameter ϵ_1 at $\phi = \phi_k$ as

$$\epsilon_1 = \frac{2\alpha - 1}{(2\alpha - 1) + 2N_k(\alpha - 1)}. \tag{107}$$

Putting Eq. (107) and Eq. (103) into Eq. (17), we get the expression for the spectral index

$$n_s = 1 - 2\frac{(3\alpha - 2)}{(2\alpha - 1) + 2N_k(\alpha - 1)}. \tag{108}$$

Using this equation the number of e-folds N_k can be expressed in terms of the spectral index n_s as

$$N_k = \frac{(3\alpha - 2)}{(\alpha - 1)(1 - n_s)} - \frac{(2\alpha - 1)}{2(\alpha - 1)}. \tag{109}$$

The value of the potential at the end of inflation can be expressed in terms of H_k using Eqs. (80) and (101) as

$$V_{\rm end} = 3M_P^2 H_k^2 \left[\frac{\exp\left(-\sqrt{\frac{2}{q}}\frac{\phi_{\rm end}}{M_P}\right)}{\exp\left(-\sqrt{\frac{2}{q}}\frac{\phi_k}{M_P}\right)}\right]. \tag{110}$$

Solving the above equation with Eq. (104) and Eq. (106)

$$V_{\rm end} = 3M_P^2 H_k^2 \left[\frac{2\alpha - 1}{(2\alpha - 1) + 2N_k(\alpha - 1)}\right]^{\frac{2\alpha-1}{\alpha-1}}. \tag{111}$$

The Hubble constant at $\phi = \phi_k$, can be obtained by substituting the expression for the speed of sound c_S, (85), and the slow-roll parameter ϵ_1, (107) in Eq. (15) as

$$H_k = \pi M_P \sqrt{8A_S \frac{2\alpha - 1}{(2\alpha - 1) + 2N_k(\alpha - 1)} \frac{1}{\sqrt{2\alpha - 1}}}. \tag{112}$$

Using equation Eq. (112), Eq. (110), and Eq. (109), we can obtain H_k and $V_{\rm end}$ as a function of n_s. Again, by using these expressions for H_k and $V_{\rm end}$, the reheating

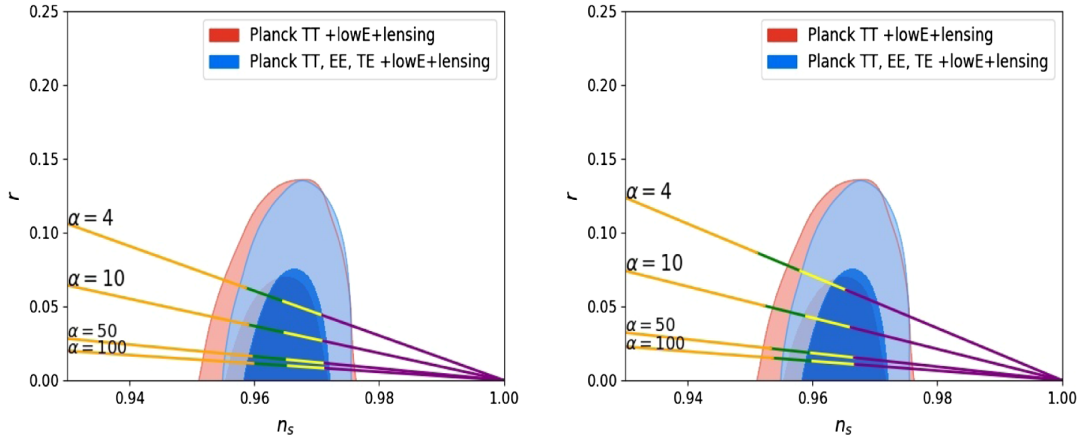

FIG. 8. r vs n_s predictions for quadratic and quartic potentials with four different choice of α along with joint 68% C.L. and 95% C.L. *Planck* 2018 constraints. Here the orange region corresponds to $w_{re} \leq 0$, the green region corresponds to $0 \leq w_{re} \leq 0.25$, the yellow region shows $0.25 \leq w_{re} \leq 1$ and the purple region corresponds to $w_{re} > 1$.

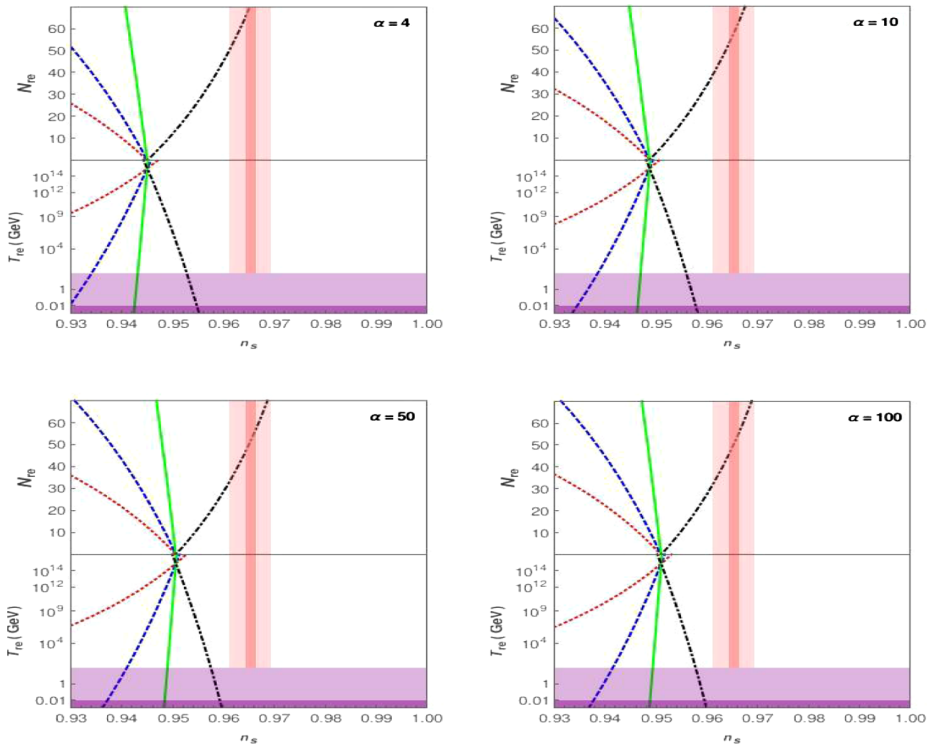

FIG. 9. N_{re} and T_{re} as function of n_s for four different values of α of the exponential potential with a power-law kinetic term. The vertical pink region shows *Planck* 2018 bounds on n_s and the dark pink region represents a precision of 10^{-3} from future observations [61]. The horizontal purple region corresponds to T_{re} of 10 MeV from BBN and the light purple region corresponds to 100 GeV of the electroweak scale. The red dotted line corresponds to $w_{re} = -\frac{1}{3}$, the blue dashed lines corresponds to $w_{re} = 0$, the green solid line corresponds to $w_{re} = 0.25$, and the black dot-dashed line is for $w_{re} = 1$.

temperature T_{re} and the number of e-folds during reheating N_{re} can be obtained in terms of n_s from Eqs. (29) and (28) respectively. The variation of N_{re} and T_{re} with respect to n_s for various choices of α and effective equation of state during reheating is shown in Fig. 9.

By demanding $T_{re} > 100$ GeV we obtain bounds on n_s using Eq. (29) for various values of w_{re}. Again from these bounds on n_s, the bounds on N_k can be obtained using Eq. (109). The tensor to scalar ratio r for the exponential potential with a power-law kinetic term can be obtained by substituting Eq. (85) and Eq. (107) in Eq. (18) as

$$r = \frac{16\sqrt{2\alpha - 1}}{2\alpha - 1 + 2N_k(\alpha - 1)}, \quad \alpha > 1. \tag{113}$$

Using this expression we can get bounds on r from the bounds on N_k, obtained by the reheating consideration.

TABLE V. The allowed values of spectral index n_s and the number of e-folds N_k for various values of α for exponential potentials with a power-law kinetic term, considering $T_{re} \geq 100$ GeV.

α	Equation of state	n_s	N_k	r
$\alpha = 4$	$-1/3 \leq w_{re} \leq 0$	$0.8888 \leq n_s \leq 0.9341$	$31.81 \leq N_k \leq 54.45$	$0.2353 \geq r \geq 0.1395$
	$0 \leq w_{re} \leq 0.25$	$0.9341 \leq n_s \leq 0.9431$	$54.45 \leq N_k \leq 63.30$	$0.1395 \geq r \geq 0.1204$
	$0.25 \leq w_{re} \leq 1$	$0.9431 \leq n_s \leq 0.9528$	$63.30 \leq N_k \leq 76.44$	$0.1204 \geq r \geq 0.0999$
$\alpha = 10$	$-1/3 \leq w_{re} \leq 0$	$0.8967 \leq n_s \leq 0.9385$	$30.1371 \leq N_k \leq 51.39$	$0.1286 \geq r \geq 0.0765$
	$0 \leq w_{re} \leq 0.25$	$0.9385 \leq n_s \leq 0.9469$	$51.39 \leq N_k \leq 59.72$	$0.0765 \geq r \geq 0.0660$
	$0.25 \leq w_{re} \leq 1$	$0.9469 \leq n_s \leq 0.9559$	$59.72 \leq N_k \leq 72.09$	$0.0660 \geq r \geq 0.0549$
$\alpha = 50$	$-1/3 \leq w_{re} \leq 0$	$0.9020 \leq n_s \leq 0.9410$	$30.01 \leq N_k \leq 50.53$	$0.0527 \geq r \geq 0.0317$
	$0 \leq w_{re} \leq 0.25$	$0.9410 \leq n_s \leq 0.9489$	$50.53 \leq N_k \leq 58.58$	$0.0317 \geq r \geq 0.0274$
	$0.25 \leq w_{re} \leq 1$	$0.9489 \leq n_s \leq 0.9575$	$58.58 \leq N_k \leq 70.54$	$0.0274 \geq r \geq 0.0229$
$\alpha = 100$	$-1/3 \leq w_{re} \leq 0$	$0.9034 \leq n_s \leq 0.9415$	$30.25 \leq N_k \leq 50.64$	$0.0366 \geq r \geq 0.0221$
	$0 \leq w_{re} \leq 0.25$	$0.9415 \leq n_s \leq 0.9493$	$50.64 \leq N_k \leq 58.63$	$0.0221 \geq r \geq 0.0192$
	$0.25 \leq w_{re} \leq 1$	$0.9493 \leq n_s \leq 0.9578$	$58.63 \leq N_k \leq 70.52$	$0.0192 \geq r \geq 0.0159$

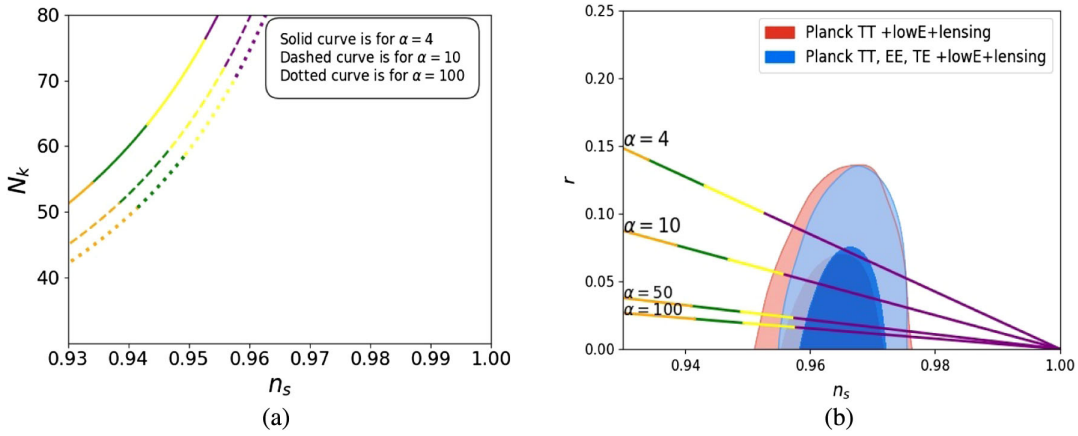

FIG. 10. In the left panel N_k as function of n_s is shown for $\alpha = 4$, 50, and 100 of exponential potentials with a power law kinetic term. In the right panel predictions of r vs n_s for exponential potentials with a power-law kinetic term along with joint 68% C.L. and 95% C.L. *Planck* 2018 constraints is shown for four choices of α ($\alpha = 4$, 10, 50, and, 100). Here, in both panels the orange region corresponds to $w_{re} \leq 0$, the green region corresponds to $0 \leq w_{re} \leq 0.25$, the yellow region shows $0.25 \leq w_{re} \leq 1$, and the purple region corresponds to $w_{re} > 1$. (a) N_k vs n_s for exponential potential for $\alpha = 4$, 10,100. (b) r vs n_s for exponential with $\alpha = 4$, 10, 50, 100.

These bounds on n_s, N_k, and r for the exponential potential are listed in Table V. It can be seen from Table V that, with $\alpha = 4$, the bounds r, i.e., $0.139 \geq r \geq 0.12$ are higher than the joint BICEP2/Keck array and *Planck* 2018 bounds $r < 0.06$ [62] for the physically plausible range $0 \leq w_{re} \leq 0.25$. However, for this range of w_{re}, the bounds on r are compatible with joint BICEP2/Keck array and *Planck* 2018 bounds for larger values of α.

The plots between N_k and n_s are shown in left panel of Fig. 10 for various values of α and w_{re}. The $r - n_s$ predictions, along with joint 68% C.L. and 95% C.L. *Planck* 2018 constraints, for this case are shown in the right panel of Fig. 10. It can bee seen from the figure that, for all values of α, the effective equation of state during reheating w_{re} should be greater than 1 to satisfy the *Planck*-2018 joint constraints on r and n_s, which violates causality.

VI. CONCLUSION

k-inflation [9,10] is an alternative to the standard single field slow-roll inflation. In this case the noncanonical kinetic term of the scalar field drives inflation. This scenario has an advantage over the canonical single field inflation as it increases the viability of various inflaton potentials, ruled out from *Planck* CMB observations, by reducing the tensor to scalar ratio. In this work we analyze models of k-inflation in the light of reheating. The phase of reheating can be parametrized in terms of three parameters, namely reheating temperature T_{re}, the effective equation of state of cosmic fluid during reheating w_{re}, and the number of e-folds during reheating N_{re}. These three parameters can be related to the amplitude of scalar perturbations, the spectral index and other inflationary parameters depending on the inflaton kinetic term and potential, and can be used to constrain models of inflation (see [50–52] for constraints on canonical single-field inflation). We derive expressions for T_{re} and N_{re} in terms of w_{re}, n_s and other inflationary parameters, and then we use these expressions to constrain models of k-inflation having a kinetic term of DBI form and power-law form. With a DBI kinetic term we choose a monomial and a natural inflation potential and with a power-law kinetic term we choose a monomial and an exponential potential. In [45] it was shown that the equation of state during reheating w_{re} should lie between 0 to 0.25 for various reheating scenarios. By imposing $0 \leq w_{re} \leq 0.25$ and demanding that the reheating temperature $T_{re} > 100$ GeV for weak-scale dark matter production, we find bounds on n_s and number of e-foldings N_k from the time when the mode k corresponding to the pivot scale, $k_0 = 0.05\ \mathrm{M_{pc}}^{-1}$ leaves the Hubble radius during inflation to the end of inflation. These bounds on n_s and N_k can be transferred the bounds on tensor to scalar ratio r, and hence the allowed region in $n_s - r$ plane for models of inflation is restricted.

The bounds obtained for N_k and r for k-inflation with a DBI kinetic term and monomial potentials $V \sim \phi^n$ are shown in Table I and the $r - n_s$ predictions for various equation of states during reheating are shown in Fig. 2. We find that the tensor to scalar ratio $r > 0.0786$ for $w_{re} \leq 1$ in case of the quartic potential, which is greater than the joint BICEP2/Keck array and *Planck* 2018 bound $r < 0.06$ [62]. The $r - n_s$ predictions for $n = 2/3$ and $n = 1$ lie within the *Planck* 2018 1σ constraints for $w_{re} < 0$. The bounds on N_k and r for natural inflation potentials are shown in Table II and the predictions for $r - n_s$ are represented in Fig. 4. We find that the natural inflation with a DBI kinetic term is compatible with *Planck* 2018 observations for the physically plausible range $0 \leq w_{re} \leq 0.25$.

In case of k-inflation with a power-law kinetic term (73) the bounds on N_k and r for quadratic and quartic potentials are shown in Table III and Table IV, respectively. We find

that, with $\alpha = 4$ for a quadratic potential, the tensor to scalar ratio $r > 0.0740$ for $w_{re} \leq 0.25$ and $r > 0.0610$ for $w_{re} \leq 1$, which is slightly greater than the joint BICEP2/Keck array and *Planck* 2018 bound $r < 0.06$ [62]. However, this potential is compatible with *Planck* 2018 bounds on r for the physically plausible range $0 \leq w_{re} \leq 0.25$ with larger values of α. The $r - n_s$ predictions for these potentials are shown in Fig. 8. It can be seen from the figure that, for these predictions to lie within *Planck* 2018 1σ constants, the reheating equation of state is $w_{re} \geq 0.25$ for quartic potential. The bounds on N_k and r for an exponential potential with a power-law kinetic term are shown in Table V. We find that, for $\alpha = 4$, the tensor to scalar ratio $0.1395 \geq r \geq 0.1204$ for the physically plausible range $0 \leq w_{re} \leq 0.25$ and $r \geq 0.0999$ for $w_{re} \leq 1$, which are much larger than the joint BICEP2/Keck array and *Planck* 2018 bounds $r < 0.06$ [62]. Again, bounds on r are compatible with *Planck* 2018 bounds for larger values of α. The $r - n_s$ predictions for exponential potential are shown in Fig 10. It is evident from the figure that, for these predictions to lie within joint 68% constraints from *Planck* 2018 observations, the effective equation of state during reheating should be greater than 1.

These models of k-inflation are well motivated from string theory, and they have similar $r - n_s$ predictions. By imposing constraints from reheating we can remove this degeneracy. In [53,68] it is shown that the spectrum of gravitational waves generated during inflation is sensitive to the equation of state during reheating. We find different allowed values of w_{re} for different models to satisfy joint 68% C.L. and 95% C.L. constraints on $r - n_s$ from *Planck* 2018 observations. Hence, our analysis with future detection of gravitational waves can help us to find suitable model of inflation with a noncanonical kinetic term.

[1] A. H. Guth, Phys. Rev. D **23**, 347 (1981).
[2] V. F. Mukhanov and G. V. Chibisov, JETP Lett. **33**, 532 (1981).
[3] A. A. Starobinsky, Phys. Lett. **117B**, 175 (1982).
[4] A. H. Guth and S.-Y. Pi, Phys. Rev. D **32**, 1899 (1985).
[5] G. F. Smoot, C. L. Bennett, A. Kogut, E. L. Wright, J. Aymon, N. W. Boggess, E. S. Cheng, G. De Amici *et al.*, Astrophys. J. **396**, L1 (1992).
[6] E. Komatsu *et al.* (WMAP Collaboration), Astrophys. J. Suppl. Ser. **192**, 18 (2011).
[7] Y. Akrami *et al.* (Planck Collaboration), Astron. Astrophys. **641**, A10 (2020).
[8] J. Martin, C. Ringeval, and V. Vennin, Phys. Dark Universe **5–6**, 75 (2014).
[9] C. Armendariz-Picon, T. Damour, and V. F. Mukhanov, Phys. Lett. B **458**, 209 (1999).
[10] J. Garriga and V. F. Mukhanov, Phys. Lett. B **458**, 219 (1999).
[11] V. F. Mukhanov and A. Vikman, J. Cosmol. Astropart. Phys. 02 (2006) 004.
[12] G. W. Gibbons, Phys. Lett. B **537**, 1 (2002).
[13] A. Sen, J. High Energy Phys. 10 (1999) 008.
[14] G. W. Gibbons, K. Hori, and P. Yi, Nucl. Phys. **B596**, 136 (2001).
[15] A. Sen, J. Math. Phys. (N.Y.) **42**, 2844 (2001).
[16] A. Sen, J. High Energy Phys. 04 (2002) 048.
[17] Y. S. Piao, R. G. Cai, X. M. Zhang, and Y. Z. Zhang, Phys. Rev. D **66**, 121301 (2002).
[18] A. Mazumdar, S. Panda, and A. Perez-Lorenzana, Nucl. Phys. **B614**, 101 (2001).
[19] P. Chingangbam, S. Panda, and A. Deshamukhya, J. High Energy Phys. 02 (2005) 052.
[20] S. Choudhury and S. Panda, Eur. Phys. J. C **76**, 278 (2016).
[21] N. C. Devi, A. Nautiyal, and A. A. Sen, Phys. Rev. D **84**, 103504 (2011).
[22] S. Li and A. R. Liddle, J. Cosmol. Astropart. Phys. 10 (2012) 011.
[23] S. Unnikrishnan, V. Sahni, and A. Toporensky, J. Cosmol. Astropart. Phys. 08 (2012) 018.
[24] N. Rashidi and K. Nozari, J. Cosmol. Astropart. Phys. 05 (2018) 044.
[25] S. Bhattacharya and M. R. Gangopadhyay, Phys. Rev. D **101**, 023509 (2020).
[26] S. Lola, A. Lymperis, and E. N. Saridakis, Eur. Phys. J. C **81**, 719 (2021).
[27] V. K. Oikonomou, Eur. Phys. J. Plus **136**, 155 (2021).
[28] A. A. Sen and N. C. Devi, Gen. Relativ. Gravit. **42**, 821 (2010).
[29] S. D. Odintsov, V. K. Oikonomou, and F. P. Fronimos, Nucl. Phys. **B963**, 115299 (2021).
[30] S. Nojiri, S. D. Odintsov, and V. K. Oikonomou, Nucl. Phys. **B941**, 11 (2019).
[31] S. D. Odintsov and V. K. Oikonomou, Classical Quantum Gravity **37**, 025003 (2020).
[32] I. D. Gialamas and A. B. Lahanas, Phys. Rev. D **101**, 084007 (2020).
[33] L. F. Abbott, E. Farhi, and M. B. Wise, Phys. Lett. **117B**, 29 (1982).
[34] A. D. Dolgov and A. D. Linde, Phys. Lett. **116B**, 329 (1982).
[35] A. Albrecht, P. J. Steinhardt, M. S. Turner, and F. Wilczek, Phys. Rev. Lett. **48**, 1437 (1982).
[36] J. H. Traschen and R. H. Brandenberger, Phys. Rev. D **42**, 2491 (1990).
[37] A. D. Dolgov and D. P. Kirilova, Sov. J. Nucl. Phys. **51**, 172 (1990).
[38] L. Kofman, A. D. Linde, and A. A. Starobinsky, Phys. Rev. Lett. **73**, 3195 (1994).
[39] L. Kofman, A. D. Linde, and A. A. Starobinsky, Phys. Rev. D **56**, 3258 (1997).

[40] B. R. Greene, T. Prokopec, and T. G. Roos, Phys. Rev. D **56**, 6484 (1997).
[41] J. F. Dufaux, G. N. Felder, L. Kofman, M. Peloso, and D. Podolsky, J. Cosmol. Astropart. Phys. 07 (2006) 006.
[42] G. N. Felder, L. Kofman, and A. D. Linde, Phys. Rev. D **59**, 123523 (1999).
[43] M. Kawasaki, K. Kohri, and N. Sugiyama, Phys. Rev. Lett. **82**, 4168 (1999).
[44] M. Kawasaki, K. Kohri, and N. Sugiyama, Phys. Rev. D **62**, 023506 (2000).
[45] D. I. Podolsky, G. N. Felder, L. Kofman, and M. Peloso, Phys. Rev. D **73**, 023501 (2006).
[46] K. D. Lozanov and M. A. Amin, Phys. Rev. Lett. **119**, 061301 (2017).
[47] K. D. Lozanov and M. A. Amin, Phys. Rev. D **97**, 023533 (2018).
[48] A. R. Liddle and S. M. Leach, Phys. Rev. D **68**, 103503 (2003).
[49] S. Dodelson and L. Hui, Phys. Rev. Lett. **91**, 131301 (2003).
[50] L. Dai, M. Kamionkowski, and J. Wang, Phys. Rev. Lett. **113**, 041302 (2014).
[51] J. B. Munoz and M. Kamionkowski, Phys. Rev. D **91**, 043521 (2015).
[52] J. L. Cook, E. Dimastrogiovanni, D. A. Easson, and L. M. Krauss, J. Cosmol. Astropart. Phys. 04 (2015) 047.
[53] S. S. Mishra, V. Sahni, and A. A. Starobinsky, J. Cosmol. Astropart. Phys. 05 (2021) 075.
[54] A. Nautiyal, Phys. Rev. D **98**, 103531 (2018).
[55] D. J. Schwarz, C. A. Terrero-Escalante, and A. A. Garcia, Phys. Lett. B **517**, 243 (2001).
[56] J. Martin and C. Ringeval, Phys. Rev. D **82**, 023511 (2010).
[57] P. H. Chavanis, Phys. Rev. D **92**, 103004 (2015).
[58] J. Martin, C. Ringeval, and V. Vennin, Phys. Rev. Lett. **114**, 081303 (2015).
[59] J. Mielczarek, Phys. Rev. D **83**, 023502 (2011).
[60] R. Easther and H. V. Peiris, Phys. Rev. D **85**, 103533 (2012).
[61] L. Amendola, S. Appleby, A. Avgoustidis, D. Bacon, T. Baker, M. Baldi, N. Bartolo, A. Blanchard, C. Bonvin, S. Borgani *et al.* Living Rev. Relativity **21**, 2 (2018).
[62] P. A. R. Ade *et al.* (BICEP2 and Keck Array Collaborations), Phys. Rev. Lett. **121**, 221301 (2018).
[63] K. Freese, J. A. Frieman, and A. V. Olinto, Phys. Rev. Lett. **65**, 3233 (1990).
[64] F. Lucchin and S. Matarrese, Phys. Rev. D **32**, 1316 (1985).
[65] J. J. Halliwell, Phys. Lett. B **185**, 341 (1987).
[66] J. Yokoyama and K. I. Maeda, Phys. Lett. B **207**, 31 (1988).
[67] L. P. Chimento, R. Lazkoz, and M. G. Richarte, Phys. Rev. D **83**, 063505 (2011).
[68] V. Sahni, Phys. Rev. D **42**, 453 (1990).